New terrestrial cosmogenic ^{10}Be dating of the Ultima Esperanza moraine belts (52°S, Patagonia) confirm the global Last Glacial Maximum (LGM) ice lobe extent was half of the local LGM

Attila Çiner[1], Mehmet Akif Sarıkaya[1], Cengiz Yıldırım[1], Igor Girault[2], Dominique Todisco[2], Fabiana Martin[3], Luis Borrero[4], Derek Fabel[5]

1. Eurasia Institute of Earth Sciences, Istanbul Technical University, Maslak, 34469, Istanbul, Turkey

2. Département de Géographie, Université de Rouen, CNRS: UMR 6266, France

3. Centro de Estudios del Hombre Austral, Instituto de la Patagonia, Universidad Magallanes, Chile

4. Instituto Multidisciplinario de Historia y Ciencias Humanas, CONICET, Universidad de Buenos Aires, Argentina

5. Scottish Universities Environmental Research Centre, East Kilbride, Glasgow, United Kingdom

Abstract

The question over the (a)synchronicity of mountain glaciers and ice sheets fluctuations in the northern and southern hemispheres during the global Last Glacial Maximum (gLGM; 26.5-19 ka) is still debated. Patagonia, in South America, is probably one of the best places to understand the variations in climate fluctuations that gave rise to the development of numerous ice-lobes, which attained their maximum extents during diverse episodes of the last glacial cycle. Our study is focused around the Lago Aníbal Pinto area (52°00' S, 72°40' E), where several moraine belts were deposited by one of the eastward-flowing southern Patagonian Ice Sheet (PIS) outlet ice-lobes; the Última Esperanza. From granitic moraine boulders,

we report eight ^{10}Be terrestrial cosmogenic nuclides (TCN) surface ages. Our weighted average age obtained from the southern part of the Río Turbio moraine belt yields 50.7 ± 2.4 ka (oldest boulder age; 53.8 ± 5.3 ka) and confirms the greatest extent of the local Last Glacial Maximum (lLGM) during Marine Isotope Stage 3 (MIS 3) in the previously dated northern moraines from the same belt. Our ^{10}Be TCN age (32.6 ± 2.2 ka) derived from the Dos Lagunas moraine, which makes up the northernmost margin of the Última Esperanza ice-lobe's Arauco advance near Cerro Benítez hill, also validates the MIS 3 deglaciation timing previously reported by earlier works. Following the formation of Arauco moraines, the Última Esperanza ice-lobe was split into three main tributaries in the south, which formed three restricted and up to now undated moraine complexes. We dated one of them, the Aníbal Pinto moraine complex, a northward-flowing tributary ice-lobe that deposited an arch-shaped moraine complex in the northern and eastern boundaries of Aníbal Pinto Lake (49 m a.s.l.). While the highest moraine yielded the oldest age (28.3 ± 2.2 ka), representing the Aníbal Pinto advance, younger ages obtained from lower ridges (weighted average age = 18.9 ± 1.0 ka; oldest boulder age = 19.0 ± 1.5 ka) suggest they were deposited under the Pinto Lake level, designating the lake regression. Overall, our age results consolidate and confirm previously published ages from the Última Esperanza ice-lobe advances in the southern PIS. Additionally, for the first time, we attribute the Aníbal Pinto moraine complex to early gLGM (MIS 2), emphasising that the gLGM was half the extent of lLGM in the Última Esperanza ice-lobe.

Keywords: Aníbal Pinto moraine, Última Esperanza ice-lobe, Patagonia, cosmogenic surface exposure dating, LGM, MIS 2, MIS 3

1. Introduction

Whether the northern and southern hemispheres mountain glaciers and ice sheets reached their maximum extents asynchronously or synchronously during the global Last Glacial Maximum (gLGM; 26.5-19 ka; Mix et al., 2001; Clark et al., 2009; Hughes et al., 2013) is still debated (e.g., Broecker, 1997; Mercer, 1984; Denton et al., 1999, 2021; Fink et al., 2006; Sutherland et al., 2007; McCarthy et al., 2008; Schaefer et al., 2015). Indeed, variations exist in climate fluctuations globally, and data might be diachronous, synchronous, or asynchronous, creating difficulties in global correlations (Hughes and Gibbard, 2013).

In the southern hemisphere, in South America, Patagonian glaciers constituted an uninterrupted ice sheet during the Last Glaciation, *c.* 2000 km long between 37°S and 56°S, known as the Patagonian Ice Sheet (PIS) (Caldenius, 1932; Clapperton, 1993; Rabassa, 2008; Rabassa and Coronato, 2009; Rabassa et al., 2022). Absolute dating over the two last decades evidence that the Patagonian Ice Sheet reached the local Last Glacial Maximum (lLGM) before the global Last Glacial Maximum (gLGM) (Evenson et al., 2009; Darvill et al., 2015a, 2017; Davies et al., 2020; García et al., 2018, 2021; Girault et al., 2022). To understand the reasons behind these interhemispheric differences and their forcing mechanisms, we need to acquire more numerical age data to refine the timing of each glacial advance. With the increasing use of terrestrial cosmogenic nuclides (TCN) exposure dating methods, terminal and lateral moraines have become primary targets in measuring the maximum ice extents and inferring a particular region's paleoclimate.

Here, we present eight ^{10}Be TCN surface exposure ages from moraines deposited by one of the eastward-flowing southern PIS's outlet glaciers, the Última Esperanza ice lobe. The new surface exposure ages from the outer moraine belts confirm that the

Ultima Esperanza ice lobe reached its maximal extent during Marine Isotope Stage 3 (MIS 3), agreeing with previous studies (Sagredo et al., 2011; García et al., 2018). Additionally, for the first time, we define the limit of the gLGM moraines of the Última Esperanza ice-lobe in its southern sector at the Lago Aníbal Pinto area. We later compare our data with neighbouring ice-lobes and southern Patagonia to appreciate the gLGM *vs* lLGM record.

2. Regional setting

Our study is focused around the Lago Aníbal Pinto area (52°00' S, 72°40' E), located on the eastern side of the Patagonian Andes, which is today composed of three ice fields; the northern Patagonian Ice Field (46.5°S to 47.5°S), the southern Patagonian Ice Field (48.5°S to 51.5°S), and the Cordillera Darwin Ice Field (54.5°S to 55.0°S) covering *c.* 19.000 km² (Davies and Glasser, 2012) (Fig. 1).

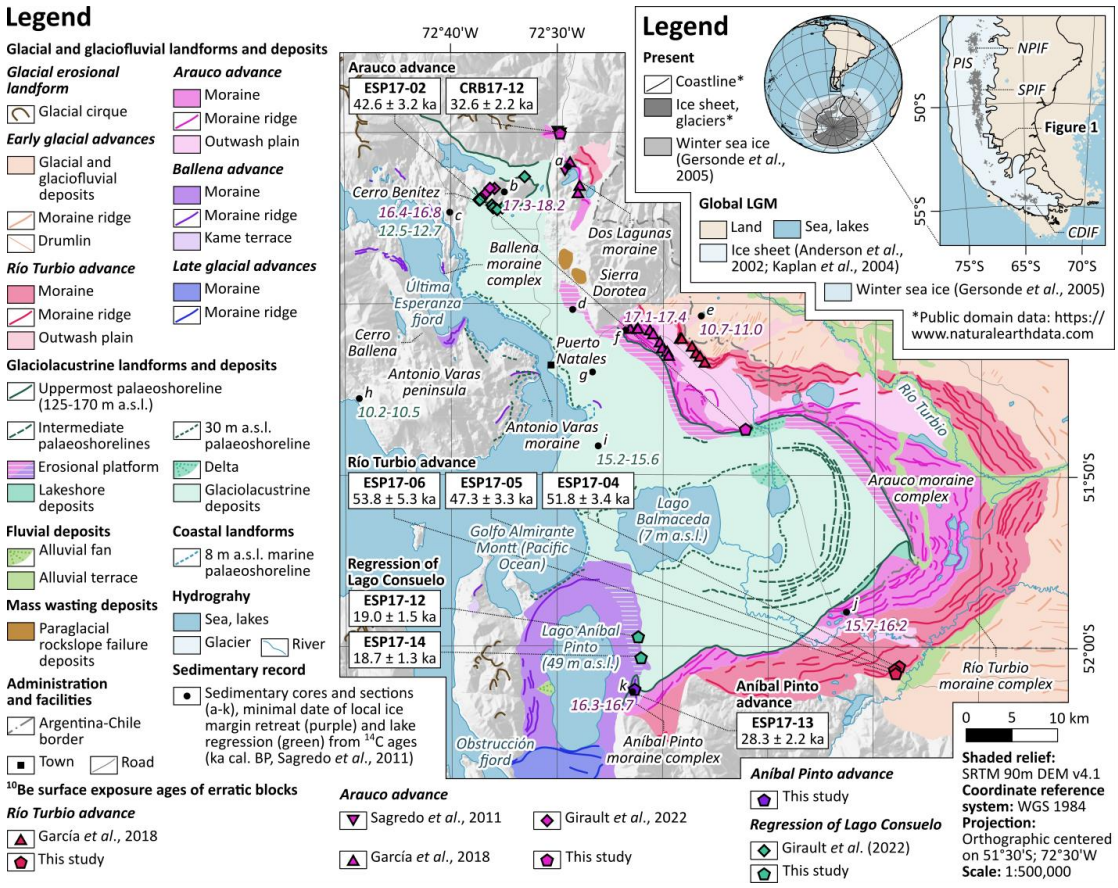

Fig. 1: Study area location and geomorphological map: Insert: Patagonian Ice Sheet extent during the gLGM and Present. B: Geomorphological map of the Última Esperanza ice-lobe moraine complexes modified from Sagredo et al. (2011), García et al. (2014, 2018) and Girault et al. (2022). Sagredo et al. (2011) cores and sections: a: Lago Dorotea pit; b: Vega Benítez pit; c: Eberhard pit; Dorotea pits section; e: Dumestre section; f: Pantano Dumestre pit; g: Lago Pintito pit.

Apart from northern Patagonia, the western outlet glaciers reached the Pacific Ocean via fjords, while their eastern counterparts terminated on land. The PIS covered an area of *c.* 500.000 km² and constituted 66 main outlet ice-lobes, 52 of which were flowing eastward (Hulton et al., 2002; Glasser et al., 2008; Davies et al., 2020). The PIS glacial chronology has been extensively studied, as it contains numerous well-preserved and accessible erratic boulders, moraine belts, and glaciolacustrine deposits (e.g. Glasser et al., 2008; Kaplan et al., 2007, 2008; Moreno et al., 2015; Hein et al., 2010, 2011, 2017; Harrison and Glasser, 2011; Boex et al., 2013; Jomelli et al., 2014; Sagredo et al., 2011; Mendelova et al., 2017; García et al., 2021). In the northern PIS, relatively thin, steep, narrow, and short mountain glaciers prevailed, while the southern PIS glaciation style was mountain ice sheets composed of thicker and more extensive ice (García, 2012). The southern PIS was the most glaciated part of the Andes Mountains and constituted a plateau with elevations ranging from 800 to 2000 m above sea level (a.s.l.), with peaks above 3000 m a.s.l. in a few places.

The precipitation and temperature regime of Patagonia is affected by the west-east topographic profile of the Andes (Carrasco et al., 2002). High precipitations (7 m/yr on the coast and 10 m/yr on the icefield; DGA, 1987) and reduced temperatures (Garreaud, 2007) are brought by westerly winds sourced from the Antarctic Polar

Front Zone. The rain shadow of the Andes causes a rapid decrease in precipitation to below 400 mm/yr in eastern Patagonia (Ibarzabal y Donangelo et al., 1996).

2.1. The Última Esperanza ice-lobe glacial advances

The Última Esperanza ice-lobe developed from the coalescence of at least seven tributary glaciers during the last glaciation and extended from the Andes towards the east (Coronato et al., 2004; Coronato and Rabassa, 2011; Sagredo et al., 2011; García et al., 2018). Moraines and erratic boulders together with kame terraces, outwash and glaciolacustrine sediments constitute the essential glacial deposits of the Última Esperanza ice-lobe. Detailed mapping and ^{14}C and ^{10}Be TCN exposure dating studies carried out by Sagredo et al. (2011), García et al. (2018), and Girault et al. (2022) underpin our understanding of the timing and the extent of these deposits (Supplementary Table 1).

Below, we briefly provide the current state of understanding regarding Última Esperanza ice-lobe deposits, using previously established ^{10}Be TCN exposure and ^{14}C geochronologies from moraine complexes and erratic boulders, and sediment cores, respectively.

2.1.1. Río Turbio moraine complex

Sagredo et al. (2011) identified two extensive, crescent-shaped moraine complexes in the eastern sector of the Última Esperanza. The outermost complex called the Turbio moraine complex (Caldenius, 1932; Meglioli, 1992; Sagredo et al., 2011) is a *c.* 100 km long arc composed of several semi-continuous moraine ridges *c.* 10 km long and 10-15 m high. Moraine ridge elevations decrease from 370 m a.s.l. in the south to 150 m a.s.l. towards its easternmost extent. Although this complex was first assigned to the penultimate glaciation or "Gotiglacial" by Caldenius (1932), García et al. (2018)

^{10}Be TCN exposure ages indicate that the Río Turbio moraine complex was deposited at 45.7 ± 1.3 ka.

2.1.2. Dos Lagunas moraine

To the northeast of Cerro Benítez hill, the Última Esperanza ice-lobe formed a 3.3 km long, 100 m high and 2 km wide arcuate moraine, named “Dos Lagunas moraine” on top of a bedrock plateau *c.* 300 m a.s.l. (Sagredo et al., 2011; García et al., 2014; Girault et al., 2022). Sagredo et al. (2011) obtained three ^{10}Be TCN exposure ages from this former ice margin position (median age = 36.0 ± 1.0 ka).

2.1.3. Arauco moraine complex

The inner complex, called the Arauco moraine complex, is composed of moraine ridges *c.* 80 km long, and in the east, they are almost parallel and concentric to the Río Turbio moraines (Sagredo et al., 2011). Even though it was first named "Lago Balmaceda moraines" (Caldenius, 1932), and later "Seno Almirante Montt drift" (Meglioli, 1992), the name "Arauco moraine complex" was coined by Sagredo et al. (2011), referring to the local "Cordón Arauco" (Arauco belt).

The Arauco moraines’ outer ridges are well preserved and are as high as Río Turbio moraines. However, its inner margin is highly eroded by wave action below 125-170 m a.s.l., and moraine heights are lower (Sagredo et al., 2011). ^{10}Be TCN ages yield a deglaciation age of 32.4 ± 1.1 ka (García et al., 2018). Consistently, Girault et al. (2022) demonstrated that the northern extremity of the Ultima Esperanza ice lobe retreated from the Dos Lagunas moraine between 36.9 and 31.9 ka from chronological modelling based on ^{10}Be TCN surface exposure ages of four erratic blocks deposited on Cerro Benítez hill from 512 m a.s.l. to 218 m a.s.l. (Fig. 1).

2.1.4. Lago Aníbal Pinto moraine complex

After the deposition of Arauco moraines, the Última Esperanza ice-lobe split into three main tributaries, which formed three up to now undated moraine complexes.

In the south, a northward-flowing tributary ice-lobe, named Aníbal Pinto moraine complex, deposited an arch-shaped moraine complex (28 km long, 3 km wide and up to *c.* 100 m high) at 150 m a.s.l. in the northern and eastern boundaries of Aníbal Pinto Lake (49 m a.s.l.) (Sagredo et al., 2011) (Fig. 2a). The moraine belt is flattened at the top up to 170 m a.s.l. due to wave erosion. Boulders frequently occur as clusters accumulated by lacustrine erosion. Above this level, 15-20 m high ridges contain boulders up to 3 m in height (Fig. 2b). Striated surfaces on a rocky slope are exposed in the lake's southeastern part at an elevation between *c.* 200-400 m a.sl. (Fig. 2c).

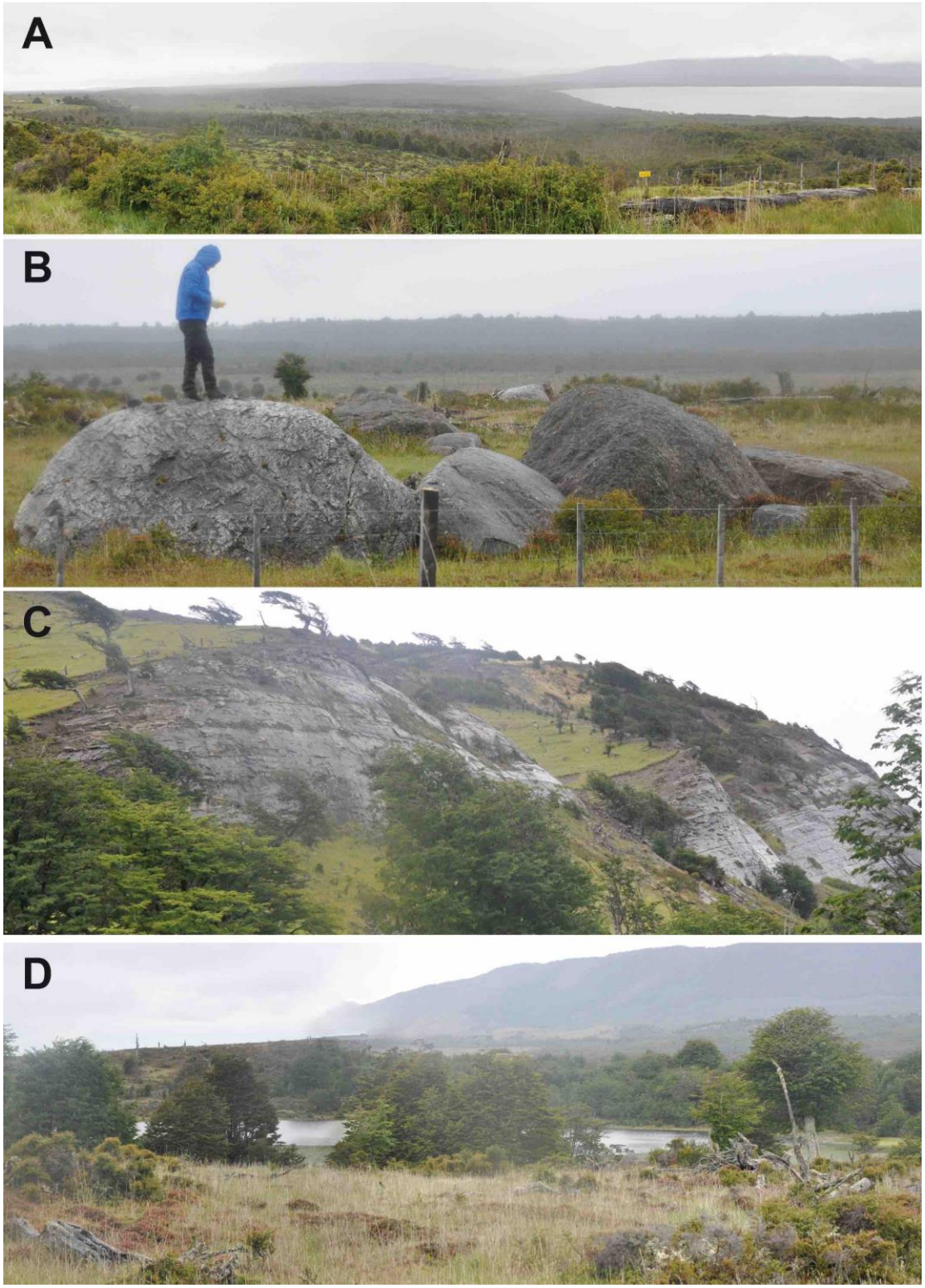

Fig. 2: Field pictures from Aníbal Pinto moraine complex: A) Aníbal Pinto Lake view towards the southwest. B) Boulder trains composed of erratics on flattened moraine surface. C); Glacially sculpted bedrock wall. D) Lago Pintito, a small lake developed after the ice retreat in between moraine ridges.

2.1.5. Antonio Varas and Cerro Ballena moraine complexes

The Antonio Varas moraine complex comprises two east-west discontinuous moraines up to 20 m high. It was deposited by a western, eastward-flowing tributary ice-lobe on both sides of the Última Esperanza fjord near Puerto Natales 40 m below sea level, indicating sub-aqueous sedimentation (Sagredo et al., 2011).

Another northwestern, eastward-flowing tributary ice-lobe deposited two 4 km long and *c.* 60 m high moraines on the northern shore of the Antonio Varas Peninsula, previously represented by Glasser et al. (2008), as part of a wider moraine arc extending on both sides of the fjord recently mapped and named "Cerro Ballena moraine complex" by Girault et al. (2022).

2.2. Rise and fall of Lago Consuelo

2.2.1. Lake level fluctuations

After the Ultima Esperanza ice lobe retreated from the Arauco moraine complex, an ice-dammed lake named “Lago Consuelo” filled the depression delimited by the ice margin, to the west, and by moraines, to the east, north and south (Moreno, 1899; Caldenius, 1932; Sagredo et al., 2011; Stern et al., 2011). The result was the development of an extensive glaciolacustrine land system composed of erosional platforms, deltas, lakeshore deposits, and palaeoshorelines (Garcia et al., 2014; Girault et al., 2022). A channel cut marks the initial lake level through the Arauco moraine complex that drained the lake to the Atlantic Ocean and rose westward due to post-glacial isostatic rebound, up to 170 m a.s.l. (Stern et al., 2011; Girault et al., 2022). As the ice margin retreated, the lake experienced a chain of drainage reversals from north to the south. First, the Tehuelche Lake drained to Lago Consuelo, lowering its level to 150-165 m a.s.l. (Solari et al., 2012), then Lago Consuelo drained to the Magallanes Lake

system, 20-30 m a.s.l., which eventually drained to the Pacific Ocean (Kilian et al., 2013).

2.2.2. Chronology of the lake regression

Until recently, the chronology of the lake regression was known only from ^{14}C dates on organic glaciolacustrine and peat deposits, indicating minimal date of ice margin retreat and lake regression, respectively. Sagredo et al. (2011) conducted an extensive drilling campaign and obtained sediment cores from several lakes formed after the withdrawal of the Última Esperanza ice-lobe (Fig. 1). The oldest ^{14}C age comes from the organic glaciolacustrine sediments of Vega Benítez (215 m a.s.l.) (Fig. 1), which yielded a minimum glacier retreat age of 17.5 ± 0.6 ka cal. BP. Similar ages were obtained from other lakes, such as 16.9 ± 0.4 ka cal. BP from Lago Dorotea (260 m a.s.l.), and 16.4 ± 0.4 ka cal. BP from Eberhard Lake (68 m a.s.l.). Lago Pintito (172 m a.s.l.), a small lake that formed in an intermorainal depression of the Aníbal Pinto moraine complex, is dated to 16.3 ± 0.4 ka (Sagredo et al., 2011) (Fig. 2d). Younger ^{14}C ages from peats above lacustrine sediments yielded minimum lake drainage ages of 15.2 ± 0.3 ka cal. BP, and 12.8 ± 0.2 ka cal. BP from Pantano Dumestre (77 m a.s.l.) and Eberhard Lake (68 m a.s.l.), respectively. In addition, ^{14}C age of the earliest megafaunal material found in the lakeshore caves of Cerro Benítez dated to 18.2 ± 0.3 ka cal. BP in Cueva Chica (Martin et al., 2013) inferred that the lake had already fallen at that time from its uppermost level (Girault et al., 2022).

More recently, Girault et al. (2022) ^{10}Be TCN dated seven erratic blocks deposited on the upper erosional platform of Lago Consuelo surrounding Cerro Benítez, between 148 and 136 m a.s.l. Considering that the surface exposure ages indicate the lowering of the lake level, the ^{10}Be TCN surface exposure ages recalculated with a chronological model suggest that the platform locally emerged as a result of post-glacial isostatic

rebound between 21.7 and 16.9 ka, and drainage reversal to the Magallanes Lake system occurred between 16.9 and 15.4 ka.

3. Methodology

3.1. Fieldwork and mapping

We used the recently published geomorphological map of Girault et al. (2022), based on remote sensing and field data and revision of the previous works of Sagredo et al. (2011) and García et al. (2018). A total of four field seasons, each at least one month, were needed to complete mapping and sampling.

3.2. Terrestrial cosmogenic nuclide (TCN) dating of moraine boulders

3.2.1. Rationale

We used the ^{10}Be (half-life of 1.387 ± 0.012 Ma, Korschinek et al., 2010) TCN surface exposure dating method to infer moraine boulder exposure ages, which were deposited by a retreating glacier (Stone et al., 2003). Our samples contain enough quartz to measure *in-situ* ^{10}Be, which is ideal for dating Quaternary glacial deposits. As the production rate of *in-situ* produced cosmogenic ^{10}Be is known (Kaplan et al., 2011; Borchers et al., 2015; Lifton et al., 2014), the measured ^{10}Be concentrations in boulders yield the exposure duration. ^{10}Be TCN surface dating became the dominant method for reconstructing the PIS chronology since its first use in the region by Kaplan et al. (2004). The method has increased our understanding of Patagonian glaciers' waxing and waning, specifically the Última Esperanza ice-lobe (Sagredo et al., 2011; García et al., 2018; Girault et al., 2022).

3.2.2. Sample collection

We collected a total of 12 granitic moraine boulder samples. We aimed at the areas that previous researchers have not sampled. We used a chisel and hammer for the sample collection from the uppermost few centimetres of the boulders. We recorded their GPS locations, topographic shielding attributes and sampled thicknesses in the field (Table 1).

We collected *c.* 1 kg of rock chips from the surface of each boulder. All collected boulders display well-developed polish and striations demonstrating glacial transportation. Out of 12 samples, four did not yield a sufficiently large amount of quartz, denoting that >1 kg of rock chips is required for the granitic lithologies we sampled.

3.2.3. BeO extraction

We first crushed and sieved the rock samples to 0.25-0.71 mm grain size at Istanbul Technical University's ITU/Kozmo-Lab (www.kozmo-lab.itu.edu.tr/en). We rinsed the crushed samples with milli-Q water, leached them overnight with a 10 % HNO_3 solution, and used a Frantz magnetic separator to collect non-magnetic minerals. We separated and purified the quartz by froth flotation, boiling in $H_4P_2O_7$ solution, and used a mixture of 2% HF-HNO_3 solution to leach quartz grains in an ultrasonic bath at the SUERC (Scottish Universities Environmental Research Centre), United Kingdom. Quartz purity was assessed by measuring the amount of native Al in the sample by ICP-OES. All samples yielded Al concentrations less than 130 mg/g. We added 222 µg ^{9}Be and dissolved the purified quartz (between 1 and 18 g) in a mixture of concentrated HF and HNO_3. Once the quartz was entirely dissolved, BeO was extracted following the methods described in Glasser et al. (2009).

3.2.4. Be isotope ratio measurements

We measured Be isotope ratios with the 5 MV Tandem Accelerator Mass Spectrometer (AMS) at the SUERC AMS Laboratory in Scotland (Xu et al., 2010). Measured $^{10}Be/^{9}Be$ values of each sample were normalised and blank corrected with the $^{10}Be/^{9}Be$ ratio of the 07KNSTD AMS standard and three full chemistry procedural blanks with an average $^{10}Be/^{9}Be = 5.502 \pm 0583 \times 10^{-15}$. Corrected isotope ratios were converted to ^{10}Be concentrations per gram of quartz.

3.2.5. Exposure age calculation

We calculated the ages using the production rates specified by the CRONUS Earth Web Calculator v3 (https://hess.ess.washington.edu; Balco et al., 2008) with the mean attenuation length of 152.1 g/cm^2. We used the Lifton-Sato flux, time-dependent scaling scheme (known as LSDn or SF) established by Lifton et al. (2014). We assumed sample density as 2.65 g cm^{-3} and applied corrections for sample thickness and topographic shielding. We did not sample weathered surfaces and report the ages without erosion correction. As past snowfall amounts are unknown, we have assumed no snow shielding, in agreement with previous authors (Sagredo et al., 2010; Garcia et al., 2018; Davies et al., 2020). Different production rates (Kaplan et al., 2011) and scaling schemes change the results by less than 10%. All essential information, including the ^{10}Be concentrations and scaling factors to reproduce resultant ages, are given in Table 1. All ancillary data to recalculate the TCN exposure ages are listed in Supplementary Table 2.

Table 1: Cosmogenic age data used in this study. Ages have been calculated using the online exposure age calculator formerly known as the CRONUS Earth Web

Calculator v3 (https://hess.ess.washington.edu; Balco et al., 2008) with the mean attenuation length of 152.1 g/cm^2, rock density of 2.65 g/cm^3 and the Lifton/Sato flux, time and nuclide-dependent scaling scheme (known as LSDn, or SA) based on Lifton et al. (2014). Choice of a different scaling scheme (i.e., Lal/Stone time-independent, ST) (Lal, 1991; Stone, 2000) would make the ages <2.4% older. Procedural blank correction applied. No snow or erosion correction was applied. Isotope ratios were referenced to the 07KNSTD standard.

Sample	Glacial stage (or event)	Latitude WGS-84	Longitude WGS-84	Elevation	Thickness	Topographic shielding factor	Quartz dissolved	^{10}Be conc.	1 σ error	**^{10}Be age**	1 σ error^{int}	**1 σ error$^{ext.}$**	**Weighted average age**
		(S)	(W)	(m asl)	(cm)	unitless	(g)	(at g^{-1})	(at g^{-1})	**(ka)**	(ka)	**(ka)**	**(ka)**
ESP17-04	Rio Turbio advance	-52.0187	-71.9592	206	2	1	14.539	285000.7	7166.6	**51.8**	1.3	**3.4**	
ESP17-05	Rio Turbio advance	-52.0220	-71.9667	214	3	1	5.203	261189.8	9546.4	**47.3**	1.8	**3.3**	**50.7 ± 2.4**
ESP17-06	Rio Turbio advance	-52.0257	-71.9648	198	1	1	0.964	295813.4	22498.3	**53.8**	4.2	**5.3**	
ESP17-02	Arauco advance*?	-51.7887	-72.2039	184	4	1	3.378	226235.6	9814.3	***42.6****	*1.9**	***3.2****	
CRB17-12	Arauco advance (Dos Lagunas)	-51.5008	-72.4957	266	1.5	0.999	6.948	189026.9	5657.8	**32.6**	1.0	**2.2**	
ESP17-12	Regression of Lago Consuelo	-51.9909	-72.3721	145	2	1	7.884	98169.3	4667.2	**19.0**	0.9	**1.5**	**18.9 ± 1.0**
ESP17-14	Regression of Lago Consuelo	-52.0113	-72.3676	169	2	1	9.677	98812.6	3762.9	**18.7**	0.7	**1.3**	
ESP17-13	Anibal Pinto advance	-52.0420	-72.3776	188	3	0.999	10.290	152086.0	7656.0	**28.3**	1.4	**2.2**	

4. Results

We obtained eight ^{10}Be TCN exposure ages on boulders from different moraines (Table 1; Fig. 3). Three boulders originate from the southern part of the Río Turbio moraine complex, a sector nearby Río Rubens that was mapped (Sagredo et al., 2011; García et al., 2018), but not previously dated. Samples ESP17-04 (206 m a.s.l.), ESP17-05 (214 m a.s.l.), and ESP17-06 (198 m a.s.l.) yielded ages of 51.8 ± 3.4 ka, 47.3 ± 3.3 ka, and 53.8 ± 5.3 ka, respectively.

Fig. 3: Erratic boulder samples and their corresponding ^{10}Be TCN ages.

We sampled another boulder on top of a moraine ridge to the northeast of Lago Balmaceda, possibly belonging to the Arauco moraine complex. Sample ESP17-02

(184 m a.s.l.) yielded an age of 42.6 ± 3.2 ka. We also collected a boulder (CRB17-12 at 266 m a.s.l.) on the Dos Lagunas moraine to the north that gave an age of 32.6 ± 2.2 ka.

Our last three samples come from the Aníbal Pinto moraine complex. One of the samples (ESP17-13; 188 m a.s.l.) was collected from a moraine ridge near Lago Pintito and gave an age of 28.3 ± 2.2 ka. This sample is 19 m and 43 m higher than the other two samples (ESP17-12; 145 m a.s.l. and ESP17-14; 169 m a.s.l.) collected from the flattened top of the moraine complex, which yielded 19.0 ± 1.5 ka, and 18.7 ± 1.3 ka, respectively.

5. Discussion

5.1. Interpretation of ^{10}Be TCN chronology

Out of eight boulders sampled, seven yielded meaningful ages that consolidate and confirm previously published age data (Fig. 4). We propose a new chronology for the Aníbal Pinto moraine complex. García et al. (2018) used median and associated median absolute deviation while reporting their ages. We preferred to use the weighted average age of boulders representing the landform age and give the oldest boulder age in parenthesis for comparison purposes.

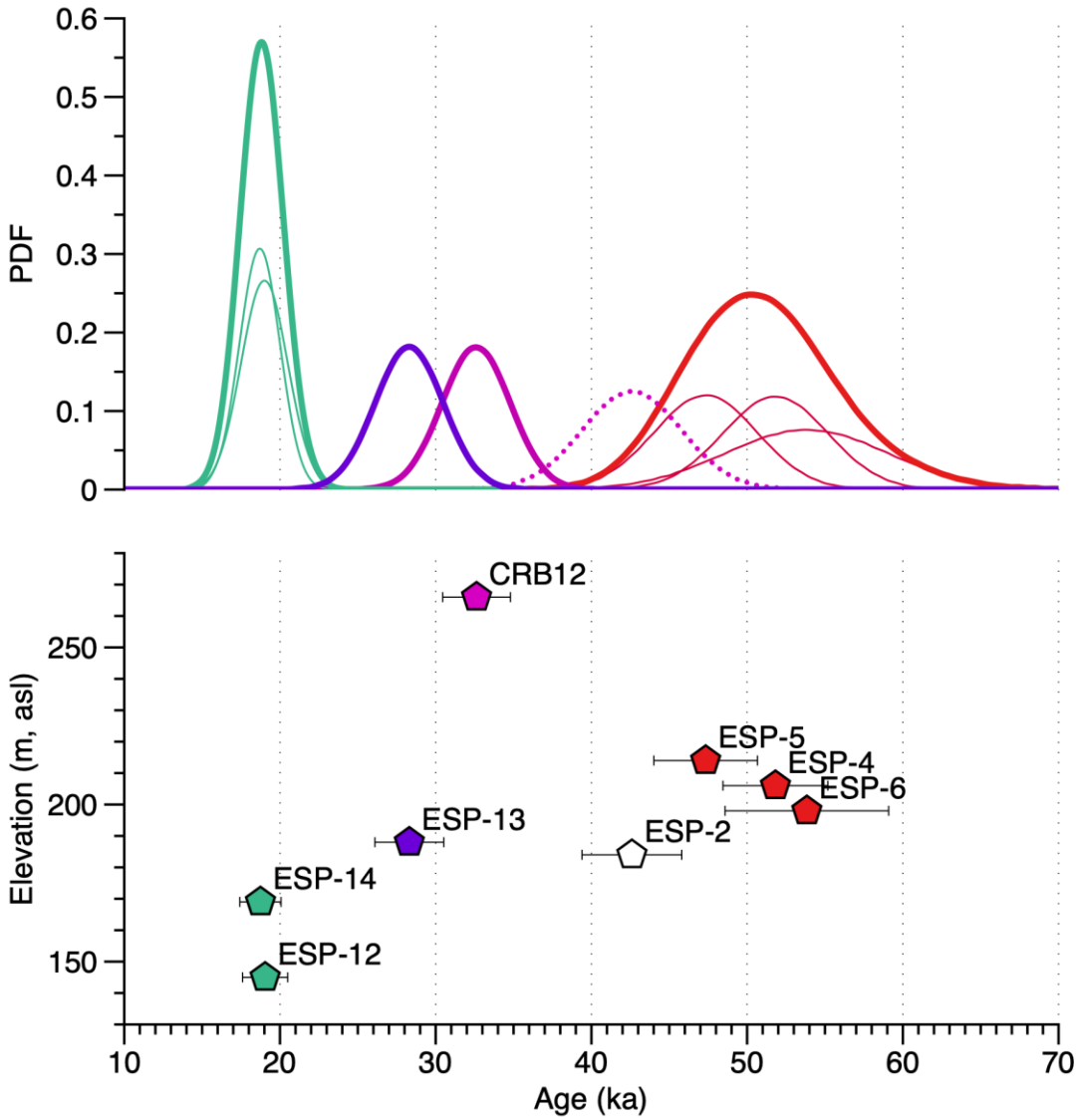

Fig. 4: Moraine boulder ^{10}Be TCN exposure ages *vs* elevation graph (lower part). Probability density function (PDF) showing the weighted average age of the exposure events (upper part). Coloured thin lines are individual ages from corresponding moraines (see map), and the coloured thick line is the summed probability curve. Purple: Río Turbio; Dashed pink: Arauco (outlier); Pink: Dos Lagunas (Arauco); Light brown: Cerro Benítez (Aníbal Pinto).

The age obtained to the northeast of Lago Balmaceda from the sample ESP17-02 (42.6 ± 3.2 ka) is older than the Arauco moraine complex median age (32.4 ± 1.1 ka), but younger than the Río Turbio moraine complex median age (45.7 ± 1.3 ka), both

provided by García et al. (2018). García et al. (2018) also collected a sample (AR-13-10) only 3 km to the east of our sample within the Arauco moraine complex. The age of this boulder (44.1 ± 3.0 ka) is comparable with our sample within their error ranges. However, García et al. (2018) considered their sample (AR-13-10) as an outlier and did not take it into account during their median age calculations.

We propose three possibilities to explain our sample's (ESP17-02: 42.6 ± 3.2 ka) age. The first would include this boulder within the innermost part of the Río Turbio moraine complex, close to its median age (45.7 ± 1.3 ka). However, a well-developed outwash plain separates the Río Turbio and the Arauco moraine complexes, and hence this alternative is less likely. The second alternative would incorporate this boulder into one of the Arauco moraine complex's external lobes (median age: 32.4 ± 1.1 ka), although its age would be too old. However, as García et al. (2018) suggested, the Última Esperanza ice-lobe might have occupied its ice-marginal position multiple times, forming composite moraines with different ages.

The third option is that the significantly older age of the sample than the median of the moraine belt could reflect inheritance either from older glacial deposits or from supraglacial transportation (see Darvil et al., 2015b on Tierra del Fuego boulder trains). Indeed, García et al. (2018) reported several old outliers collected from the Arauco moraines. Therefore, we prefer the last of these three hypotheses and exclude this boulder age from our calculations.

The boulder age (CRG17-12: 32.6 ± 2.2 ka) collected from the Dos Lagunas moraine to the north is statistically indistinguishable from the two ages (HUG-05-02: 34.7 ± 1.9 ka and HUG-05-03: 36.0 ± 2.2 ka) that Sagredo et al. (2011) obtained from the same moraine ridge. This moraine constitutes the northernmost margin of the Última Esperanza ice-lobe Arauco advance that also overrode the nearby Cerro Benítez hill.

Chronological modelling using Bayesian statistics suggests that the deglaciation most probably occurred between 36.9 ka and 31.9 ka, i.e. a 300 m ice surface lowering in 5000 years (Girault et al., 2022).

The three samples from the Aníbal Pinto moraine complex fall into two age groups; 28.3 ± 2.2 ka and 18.9 ± 1.0 ka. The highest moraine sample, which also gives the oldest age (ESP17-13; 28.3 ± 2.2 ka), could be interpreted in two ways. The first hypothesis relates the sample's old age to inheritance pertaining to an earlier glaciation. The second hypothesis, which we prefer, implies that the sample belongs to a moraine ridge deposited during the Aníbal Pinto advance at the onset of the early gLGM, after the Arauco advance dated to 32.4 ± 1.1 ka by García et al. (2018). The second hypothesis is consistent with the results of Bayesian modelling in Cerro Benítez, which indicate that the ice lobe had already retreated between 36.9 and 31.9 ka (Girault et al., 2022).

The weighted average age of the remaining two samples collected from the Aníbal Pinto moraine complex lower ridges is 18.9 ± 1.0 ka (the oldest boulder age = 19.0 ± 1.5 ka). The younger ages obtained from these two boulders suggest that they were deposited under the lake level, representing the lake regression.

In the absence of surface exposure ages, García et al. (2018) mapped the Aníbal Pinto moraine complex as part of the Arauco moraine complex. However, our ^{10}Be TCN age data suggest that the Aníbal Pinto moraine complex results from the early gLGM extent of the southernmost Última Esperanza ice-lobe (Aníbal Pinto advance), in agreement with the interpretation of Sagredo et al. (2011) and Girault et al. (2022) based on the relative position of the moraine complexes.

5.2. Local to global LGM development of the Última Esperanza ice-lobe

The lLGM extent of the northern sector of the Última Esperanza ice-lobe is represented by the Río Turbio moraine complex, centred *c.* 45.7 ± 1.3 ka, as pointed out by García et al. (2018). Our ^{10}Be TCN exposure weighted average age (50.7 ± 2.4 ka) from the southern sector of the Última Esperanza ice-lobe confirms this maximum local extent (Fig. 5.1).

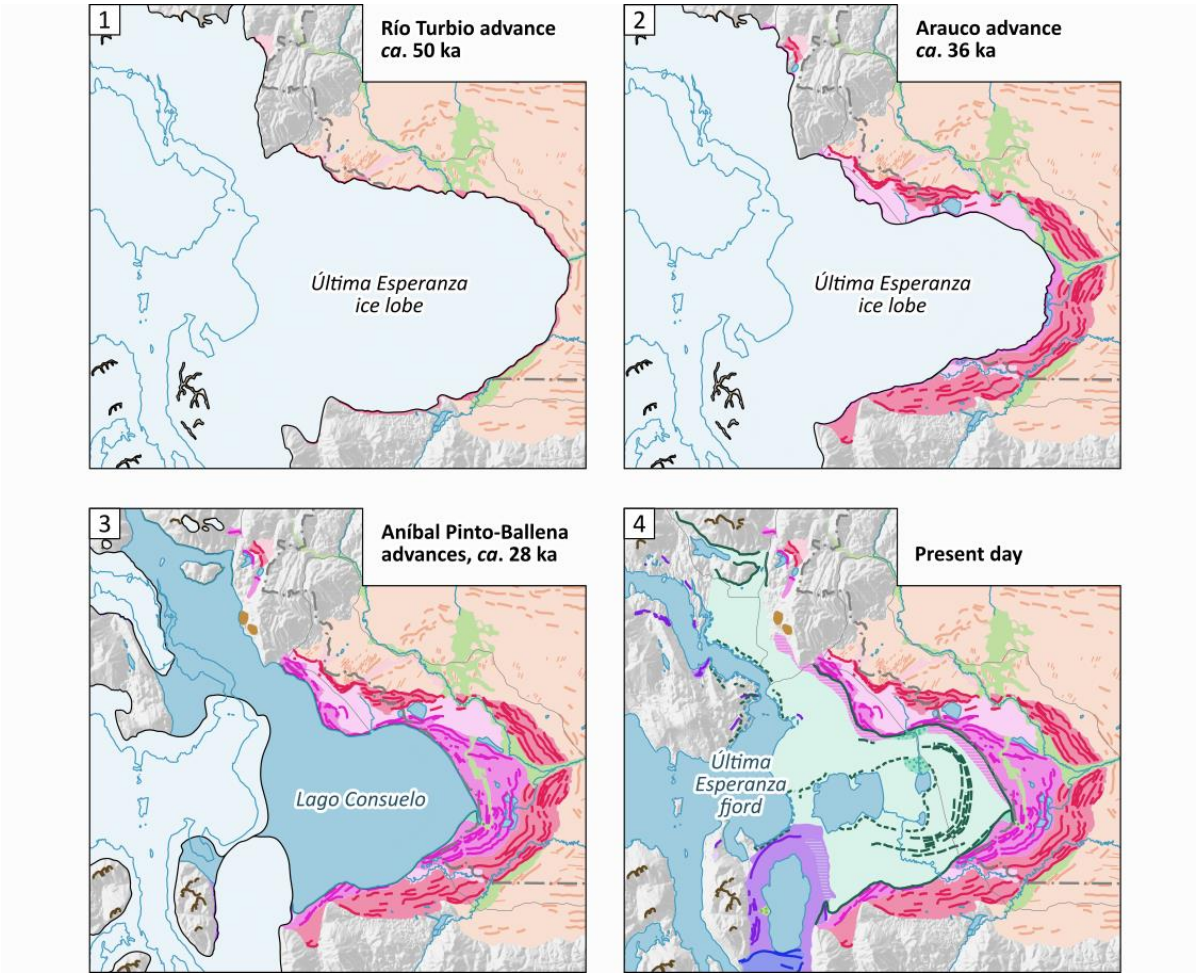

Fig. 5: Deglaciation scenario of the Última Esperanza ice-lobe from local to global LGM. For Legend see Fig. 1. 1) lLGM Río Turbio advance: 50.7 ± 2.4 ka (45.7 ± 1.3 ka; García et al., 2018). 2) Arauco advance (32.4 ± 1.1 ka; García et al., 2018), including the deposition of the Dos Lagunas moraine: (32.6 ± 2.2 ka; this study and 36.0 ± 1.0 ka; Sagredo et al., 2011). 3) Probable synchronous development of the Cerro Ballena moraine complex and the Aníbal Pinto moraine complex (28.3 ± 2.2

ka; this study) in the south. 4) Total drainage of Lago Consuelo showing the present-day topography.

Following the lLGM, the Última Esperanza ice-lobe second significant advance, the Arauco advance (Sagredo et al., 2011), is less pronounced and dated to 32.4 ± 1.1 ka by García et al. (2018) (Fig. 5.2). This advance also deposited the Dos Lagunas moraine (36.0 ± 1.0 ka, García et al., 2018; and 32.6 ± 2.2 ka, this study) in the northern sector.

Following the Arauco advance, the partial retreat of the Última Esperanza ice-lobe from the area gave rise to the development of an ice-dammed proglacial lake, Lago Consuelo (Fig. 5.3). The surface exposure age of the only dated erratic block on the Pinto moraine complex located above the uppermost lake level, hence not dating the lake regression, is 28.3 ± 2.2 ka (ESP17-13).

The Cerro Ballena moraine complex is undated and might remain so in the future, considering that this moraine complex is most probably deposited under the contemporary lake level. Therefore, surface exposure ages from its top would date the lake regression. Hence, whether the Pinto and Ballena advances occurred in synchronicity or not remains speculative. In the Torres del Paine ice lobe area, *c.* 20 km to the north, Garcia et al. (2018) dated the Torres del Paine I (TDPI) moraine complex *c.* 21.5 ka, based on the ^{10}Be TCN surface exposure age of five erratic blocks. Comparing the glacial advances to respective extents, Girault et al. (2022) suggested that the Ballena and TDPI advances occurred synchronously.

Pinto moraine complex was probably deposited synchronously with the TDPI advance. The slightly older surface exposure age of ESP17-13 (28.3 ± 2.2 ka) might be due to inherited surface exposure before deposition. Alternatively, it is conceivable that the surface exposure age of ESP17-13 primarily reflects the ice margin retreat

from the Lago Pinto moraine complex. In this case, the glacial readvance in the Ultima Esperanza and Torres del Paine ice lobes area would have occurred in a narrow time interval spanning the MIS 2 and mostly the gLGM (19.0-26.5 ka; Clark et al., 2009).

The Última Esperanza ice-lobe readvance had roughly the same magnitude as the Torres del Paine ice-lobe, i.e. *c.* 50 km inboard of their respective outer moraines, formed *c.* 100 km east of the southern PIS. All data presented above confirm that the gLGM (MIS 2) was half the lLGM (MIS 3) extent in south Patagonia.

5.3. The Patagonian local (MIS 3) *vs* global (MIS 2) LGM

A detailed discussion on the Patagonian local and global LGM ice extents is presented in García et al. (2018), and thus it is not the aim of this section to repeat a similar debate. However, in the light of the new TCN ages, it is worth adding similarities and differences, which will help better understand the gLGM in Patagonia.

Although earlier dates obtained from Patagonia moraines designate an MIS 2 glaciation (Denton et al., 1999; Kaplan et al., 2004, 2008; Sudgen et al., 2005; McCulloch et al., 2005; Hein et al., 2010; Moreno et al., 2015; Darvill et al., 2016), there is increasingly robust evidence suggesting the existence of a maximum ice extent during MIS 3 (*c.* 57-29 ka), MIS 4 (*c.* 71-57 ka) (Doughty et al., 2021) and even MIS 5 (*c.* 130-80 ka).

Mendelova et al. (2020) provided the oldest glaciation timing from moraine and glacial outwash ^{10}Be TCN ages from the Lago Belgrano area in central Patagonia. They concluded that the most widespread glacial development occurred at *c.* 75 ka, at the end of MIS 5.

Recently, Peltier et al. (2021) delivered the first direct dating of MIS 4 glaciation (*c.* 68 ka) from the Magallanes ice-lobe in southernmost Patagonia, Chile. This most significant expansion lasted until *c.* 62 ka, denoting a hemispheric and probably global phenomenon similar to MIS 2. Besides glaciers, i.e. pollen records (Heusser et al., 1999) and sediment cores from the southeast Atlantic Ocean (Barker and Diz, 2014), proxy data also infer that MIS 4 reached at least the size of the gLGM in Patagonia. Additionally, MIS 3 reached practically the size of MIS 4 in Magellanes ice-lobe as a moraine dated to *c.* 39 ka is found at the innermost edge of MIS 4 moraine (Peltier et al., 2021).

Nevertheless, the most striking proof of an early maximum ice extent comes from ^{10}Be TCN ages provided from the Última Esperanza by Sagredo et al. (2011) in the Dos Lagunas moraine (*c.* 36 ka), and by García et al. (2018) in the Río Turbio and the Arauco moraine belts *c.* 50 ka and *c.* 34 ka, respectively. The Torres del Paine ice-lobe, only *c.* 40 km to the north of the Última Esperanza ice-lobe, has strikingly comparable ages (the RV I terminal moraine *c.* 46 ka and the RV II lateral moraine *c.* 35 ka) (García et al., 2018). The close synchrony in the advances of both ice-lobes was used by García et al. (2018) as an indication of climate forcing rather than local glacier dynamics. Some other works in the Chilean Lake District (Denton et al., 1999; Moreno et al., 2015), in the Lago San Martín area (Glasser et al., 2011), and in Río Cullen and San Sebastian glacial advances in Tierra del Fuego (Darvill et al., 2015b) also support these observations. Within error limits, the glacial expansion at *c.* 57 ka in Chiloé Island, in northwestern PIS, also indicates MIS 3 glacial conditions (García et al., 2021).

Almost 250 km south of our study site, Peltier et al. (2021) dated five moraine sets that belong to Magallanes ice-lobe with multi-century accuracy. The ages range from

c. 27 ka to *c.* 18 ka (MIS 2). All moraines were inboard of MIS 4 moraines, indicating that MIS 2 was climatically less severe. Small recessional moraine crests, deposited on a drumlinised terrain and found 18 km inboard of these MIS 2 moraines, were dated to *c.* 18 ka (Peltier et al., 2021).

5.4. Local to global LGM in southern and northern hemispheres

The question of (a)synchronous development of the mountain glaciers and ice sheets in southern and northern hemispheres during the gLGM is challenging as vast ice sheets might have complicated responses to the global record of ice volume changes. For instance, although the southeastern sector of the Fennoscandinavian Ice Sheet was synchronous with the gLGM (Hughes et al., 2013), in its southwestern sector, the maximum extent was attained earlier, in MIS 4 and MIS 3 (Houmark-Nielsen, 2011), with a significant ice advance in MIS 2 at 21-19 ka (Mangerud et al., 2011). British-Irish Ice Sheet also followed a similar pattern with different behaviours in different sectors (Clark et al., 2012).

On the other hand, several studies in the northern hemisphere indicate that gLGM was synchronous in the Alps (Monegato et al., 2017; Seguinot et al., 2018) and most of the Mediterranean region (Hughes and Woodward, 2017; Sarıkaya and Çiner, 2015, 2017). For instance, numerous examples from the eastern Mediterranean (e.g., Sarıkaya et al., 2014; Köse et al., 2019), eastern Black Sea Mountains of Turkey (Akçar et al., 2007, 2008), central Anatolia (Sarıkaya et al., 2009; Akçar et al., 2014), the Caucasus (Dede et al., 2017), Greece (Leontaritis et al., 2020), Dinarids (Çiner et al., 2019; Zebre et al., 2019, 2021; Sarıkaya et al., 2020), and Corsica (Kuhlemann et al., 2008) show that most of the glaciers were in tune with gLGM and reached their maximum extents in MIS 2, with temperatures dropping between 8 to 11°C depending on the regions (e.g., Sarıkaya et al., 2008, 2009; Hughes et al., 2013; Ünal-İmer et al.,

2015; Candaş et al., 2020). However, two essential exceptions come from the Iberian Peninsula and Morocco, where the maximum ice extents were reached between *c.* 30 and *c.* 60 ka (Oliva et al., 2019), and *c.* 50 ka, (Hughes et al., 2018, 2020) from MIS 5 to 3, respectively.

Similar gLGM synchronous trends are reported from North America (Palacios et al., 2020), although many local exceptions existed, such as Sierra Nevada (Gillespie and Molnar, 1995). However, even if the mountain and continental glaciers advanced synchronously, their maximum extents might have been related to different advances (Phillips et al., 1990). Numerous geochronological data indicate that the most extensive phase of the Laurentide Ice Sheet occurred during MIS 2 (Gosse et al., 2006), although the ice volume during MIS 4 (at *c.* 65 ka) was only *c.* 20% smaller (Stokes et al., 2012). In the Sierra Nevada, the maximum extent of the glaciers during the last glacial cycle occurred at *c.* 19 ka (James et al., 2002; Phillips et al., 2009) and rapidly disappeared in a couple of thousands of years (Gillespie and Clark, 2011). Similar MIS 2 maximum ice extent is also observed in the Rockies (Licciardi and Pierce; 2008 Thackray, 2008; Laabs et al., 2009) and at the eastern edge of the Great Basin region, where new ^{10}Be ages indicate the maximum advance of valley glaciers at 21 ka in the Wasatch Range due to decreased temperatures with little to no change in precipitation as compared to present (Quirk et al., 2020).

In the northeast Tibetan Plateau, ^{10}Be TCN age results show a lessening trend in the extent of glaciation since at least MIS 4, with no observed gLGM moraines (Rother et al., 2017). Although Dortch et al. (2013) found a robust gLGM signal at *c.* 20 ka in the Pamir and western Transhimalaya, monsoon controlled glaciers (southern and eastern Tibet Plateau) attained their maximum extents during MIS 3 (Owen et al., 2008; Owen and Dortch, 2014).

On the other hand, an increasing number of data show that mid-latitude mountain glaciers and mountain ice sheets in the southern hemisphere advanced much earlier to their most advanced positions, mainly during MIS 3 (lLGM), but also during MIS 5 (e.g., Darvill et al., 2015a; Schaefer et al., 2015; Sagredo et al., 2011; García et al., 2018; Davies et al., 2020; Mendelova et al., 2020). For instance, glacial chronologies from New Zealand (Putnam et al., 2013; Kelley et al., 2014; Doughty et al., 2015) indicate lLGM at *c.* 42 to 32 ka (MIS 3) in the southern South Island. However, in the North Island, lLGM was reached later *c.* 26.5 ka ago (Shulmeister et al., 2019) related probably to a regional phenomenon (Darvill et al., 2016) or precipitation changes associated with a northward shift in the track of the westerlies (Shulmeister et al., 2019).

There are conflicting data associated with Antarctica's deglaciation times (e.g., Anderson et al., 2002). The Antarctic ice cover pattern during the LGM is reviewed by the RAISED Consortium (2014). In West Antarctica, deglaciation from the western Amundsen Sea outer continental shelf started *c.* 22 ka ago (Smith et al., 2011; Larter et al., 2014). However, in northern Victoria Land, Rhee et al. (2019) ^{10}Be and ^{26}Al TCN dated erratic cobbles on various benches at different altitudes. They showed that the lLGM occurred during MIS 4 and that the gLGM was much smaller, questioning previous views that gLGM was synchronous. In the East Antarctic ice-sheet, terrestrial data also show that lLGM occurred before 35 ka BP (Wright et al., 2008). However, caution is needed in using TCN dating on samples originating from non-erosive cold-based ice that might yield erroneously old apparent exposure ages (Nyvylt et al., 2020). Several works in the Antarctic Peninsula also indicate that ice volumes might have been much more prominent before 35 ka (lLGM) than gLGM

(e.g., Bentley and Anderson, 1998; Hjort et al., 2003; Ingolfsson, 2014; O'Cofaigh et al. 2014).

5.5. Outlook

As briefly presented above, the question of (a)synchronous development of the mountain glaciers and ice sheets in the last glacial cycle is far from being answered. On a global scale, Patagonia seems to be the best candidate for appreciating the maximum extents of numerous ice-lobes other than during gLGM. Therefore, we need more numerical age data, mainly TCN dating, from moraines, erratic boulders and outwash sediments to better constrain the PIS maximum extents' timing. Much more severe climatic conditions that gave rise to the development of numerous ice-lobe maximum extents during MIS 3, MIS 4 and even MIS 5 (lLGMs) in the PIS and partly in New Zealand probably call to a global reason, at least in the southern hemisphere. Increasing numerical age data are also critical in understanding why the lLGM was almost double in size compared to gLGM, especially in the southern PIS.

6. Conclusions

- We present eight ^{10}Be terrestrial cosmogenic nuclides (TCN) surface exposure ages from granitic moraine boulders that belong to one of the eastward-flowing southern Patagonian Ice Sheet (PIS) outlet ice-lobes; the Última Esperanza. Our weighted average age obtained from the southern part of the Río Turbio moraine belt yield 50.7 ± 2.4 ka (oldest boulder; 53.8 ± 5.3 ka) and confirm the greatest extent of the lLGM (MIS 3) in the previously dated (45.7 ± 1.3 ka; García et al., 2018) northern moraines from the same belt.

- Our ^{10}Be TCN age (32.6 ± 2.2 ka) obtained from the Dos Lagunas moraine, which makes up the northernmost margin of the Última Esperanza ice-lobe's Arauco ad-

vance near Cerro Benítez hill, also supports the MIS 3 deglaciation timing already pointed out by Sagredo et al. (2011) (median age = 36.0 ± 1.0 ka) and Girault et al. (2022) (modelled oldest age: 36.9 ka; oldest boulder age: 37.0 ± 2.8 ka).

- After the deposition of Arauco moraines, the Última Esperanza ice-lobe was split into three main tributaries in the south, forming three restricted moraine complexes. We dated one of them, the Aníbal Pinto moraine complex, a northward-flowing tributary ice-lobe that deposited an arch-shaped moraine complex in the northern and eastern boundaries of Aníbal Pinto Lake (49 m a.s.l.). The highest moraine sample yielded the oldest age (28.3 ± 2.2 ka) demonstrating the Aníbal Pinto advance deposited shortly after the Arauco advance (32.4 ± 1.1 ka; García et al., 2018). Ice moulded and striated surfaces on a rocky cliff are also visible in the lake's southeastern part at an altitude between *c.* 200-400 m a.sl. The weighted average age of the remaining two samples collected from the Aníbal Pinto moraine lower ridges is 18.9 ± 1.0 ka (the oldest boulder age = 19.0 ± 1.5 ka). The younger ages obtained from these two boulders indicate that they were deposited under the Lago Consuelo level, representing the minimum age of lake regression.

- Our age results consolidate and confirm previously published age data from the Última Esperanza ice-lobe advances in the southern PIS. For the first time, we attribute the Aníbal Pinto moraine complex to the early gLGM (MIS 2).

- We also confirm García et al. (2018)'s results from Torres del Paine ice-lobe to the north that gLGM was half the extent of lLGM also in the Última Esperanza ice-lobe.

Acknowledgements

This work was funded by the Istanbul Technical University BAP research projects 40610 and 41612, the Chilean FONDECYT projects 1150845 and 1180272, the

French CNRS PICS project GEOCEBE, and a PhD grant from the “Institut des Amériques”. We appreciate the help provided by the National Forest Corporation (CONAF) and the rangers of the Park "Monumento Natural Cueva del Milodón".

Author contribution

Attila Çiner: Writing, Fieldwork, Surface exposure dating; Mehmet Akif Sarıkaya: Surface exposure dating, Fieldwork, Writing; Cengiz Yıldırım: Fieldwork, Surface exposure dating; Igor Girault: Geomorphological mapping, Writing, Fieldwork; Dominique Todisco: Fieldwork, Supervision; Fabiana Martin: Fieldwork; Luis Borrero: Fieldwork; Derek Fabel: Surface exposure dating.

Declaration of competing interest

We confirm that there are no known conflicts of interest associated with this publication and there has been no significant financial support for this work that could have influenced its outcome.

References

Akçar, N., Yavuz, V., Ivy–Ochs, S., Kubik, P.W., Vardar, M. Schluchter, C., 2008. A case for a downwasting mountain glacier during Termination I, Vercenik valley, northeastern Turkey. Journal of Quaternary Science, 23 (3), 273–285.

Akçar, N., Yavuz, V., Ivy-Ochs, S., Reber, R., Kubik, P.W., Zahno, C., Schlüchter, C., 2014. Glacier response to the change in atmospheric circulation in the eastern Mediterranean during the Last Glacial Maximum. Quat. Geochronol., 19, 27–41.

Akçar, N., Yavuz, V., Ivy–Ochs, S., Kubik, P.W., Vardar, M. Schluchter, C. 2007. Palaeoglacial records from Kavron Valley, NE Turkey: Field and cosmogenic exposure dating evidence. Quaternary International, 164–165, 170–183.

Anderson, J., Shipp, S., Lowe, A., Wellner, J., Mosola, A., 2002. The Antarctic Ice Sheet during the LGM and its subsequent retreat history. Quaternary Science Reviews, 21, 49–70.

Balco, G., Stone, J. O., Lifton, N. A., Dunai, T. J., 2008. A complete and easily accessible means of calculating surface exposureages or erosion rates from ^{10}Be and ^{26}Al measurements. Quaternary Geochronology, 3, 174–195.

Barker, S., Diz, P., 2014. Timing of the descent into the last Ice Age determined by the bipolar seesaw. Paleoceanography, 29 (6), 489–507.

Bentley, M.J., Anderson, J.B., 1998. Glacial and marine geological evidence for the ice sheet configuration in the Weddell Sea-Antarctic Peninsula region during the Last Glacial Maximum. Antarctic Science, 10, 309–325.

Boex, J., Fogwill, C., Harrison, S., Glasser, N.F., Hein, A., Schnabel, C., Xu, S., 2013. Rapid thinning of the late Pleistocene Patagonian Ice Sheet followed migration of the Southern Westerlies. Sci. Rep. 3, 1–6.

Borchers, B., Marrero, S., Balco, G., Caffee, M., Goehring, B., Lifton, N., Nishiizumi, K., Phillips, F., Schaefer, J., Stone, J., 2015. Geological calibration of spallation production rates in the CRONUS-Earth Project Quaternary Geochronology, 31, 188–198.

Broecker, W.S., 1997. Will our ride into the greenhouse future be a smooth one? GSA Today, 7, 1–7.

Caldenius, C., 1932. Las glaciaciones cuaternarias en Patagonia y Tierra del Fuego. Geografiska Annaler, 14, 1–164.

Candaş, A., Sarıkaya, M.A., Köse, O., Şen, Ö.L., Çiner, A. 2020. Modelling Last Glacial Maximum ice cap with Parallel Ice Sheet Model to infer palaeoclimate in south-west Turkey. J. of Quaternary Science, 935–950. doi:10.1002/jqs.3239

Carrasco, J. F., Casassa, G., Rivera, A., 2002. Meteorological and climatogical aspects of the Southern Patagonia Icefield, in: The Patagonian lcefields: a unique natural laboratory for environmental and climate change studies, G. Casassa, F. V. Sepulveda, and R. M. Sinclair, eds., Kluwer Academic Plenum Publishers, New Yark, pp. 29–41.

Çiner, A., Stepišnik, U., Sarıkaya, M.A., Žebre, M., Yıldırım, C. 2019. Last Glacial Maximum and Younger Dryas piedmont glaciations in Blidinje, the Dinaric Mountains (Bosnia and Herzegovina); insights from ^{36}Cl cosmogenic dating. Mediterranean Geoscience Reviews, 1, 1, 25–43. https://doi.org/10.1007/s42990–019–0003–4

Clapperton, C., 1993. Quaternary Geology and Geomorphology of South America. Elsevier, Amsterdam, 779 p.

Clark, C.D., Hughes, A.L.C., Greenwood, S.L., Jordan, C., Sejrup, H.P., 2012. Pattern and timing of retreat of the last British–Irish Ice Sheet. Quaternary Science Reviews, 44, 112–146.

Clark, P. U., Dyke, A.S., Shakun, J. D., Carlson, A. E., Clark, J., Wohlfarth, B., Mitrovica, J. X., Hostetler, S. W., McCabe, A. M., 2009. The Last Glacial Maximum. Science, 325, 710–714.

Coronato, A. M. J., Martínez, O., Rabassa, J., 2004. Glaciations in Argentine Patagonia, Southern South America. In: Ehlers, J., Gibbard, P. (Eds), Quaternary Glaciations: Extent and chronology. Part III: South America, Asia, Africa, Australia and Antarctica. Elsevier, Amsterdam, Developments in Quaternary Science, 2, 49–66.

Coronato, A., Rabassa, J., 2011. Chapter 51 - Pleistocene Glaciations in Southern Patagonia and Tierra del Fuego. In: Jürgen Ehlers, P.L.G., Philip, D.H. (Eds.),

Developments in Quaternary Sciences. Elsevier, pp. 715–727.

Darvill, C. M., Bentley M. J., Stokes C.R., 2015b. Geomorphology and weathering characteristics of erratic boulder trains on Tierra del Fuego, southernmost South America: implications for dating of glacial deposits. Geomorphology, 228, 382–397.

Darvill, C. M., Bentley, M. J., Stokes, C. R., Hein, A. S., Rodés, A. 2015a. Extensive MIS 3 glaciation in southernmost Patagonia revealed by cosmogenic nuclide dating of outwash sediments, Earth Planet. Sc. Lett., 429, 157–169, https://doi.org/10.1016/j.epsl.2015.07.030

Darvill, C. M., Stokes, C. R., Bentley, M. J., Evans, D. J. A., Lovell, H., 2017. Dynamics of former ice lobes of the southernmost Patagonian Ice Sheet based on a glacial landsystems approach. Journal of Quaternary Science, 32, 857–876.

Darvill, C.M., Bentley, M.J., Stokes, C.R., Shulmeister, J., 2016. The timing and cause of glacial advances in the southern midlatitudes during the last glacial cycle based on a synthesis of exposure ages from Patagonia and New Zealand. Quaternary Science Reviews, 149, 200–214.

Davies, B. J., Darvill, C. M., Lovell, H., Bendle, J. M., Dowdeswell, J. A., Fabel, D., García, J.-L., Geiger, A., Glasser, N. F., Ghe- orghiu, D. M., Harrison, S., Hein, A. S., Kaplan, M. R., Martin, J. R. V., Mendelova. M., Palmer, A., Pelto, M., Rodés, A., Sagredo, E. A., Smedley, R., Smellie, J. L., Thorndycraft, V. R. 2020. The evolution of the Patagonian Ice Sheet from 35 ka to the present day (PATICE), Earth Sci. Rev., 204, 103152, https://doi.org/10.1016/j.earscirev.2020.103152

Davies, B., Glasser, N., 2012. Accelerating shrinkage of patagonian glaciers from the little ice age (~AD 1870) to 2011. J. Glaciol., 58 (212), 1063–1084.

Dede, V., Çiçek, İ., Sarıkaya, M.A., Çiner, A., Uncu, L. 2017. First cosmogenic geochronology from the Lesser Caucasus: Late Pleistocene glaciation and rock glacier development in the Karçal Valley, NE Turkey. Quaternary Science Reviews, 164, 54–67. doi:10.1016/j.quascirev.2017.03.025

Denton, G., Heusser, C.J., Lowel, T., Moreno, P., Andersen, B., Heusser, L.E., Schluhter, C., Marchant, D., 1999. Interhemispheric linkage of paleoclimate during the last glaciation. Geogr. Ann. Ser. A Phys. Geogr., 81, 107–153.

Denton, G.H., Putnam, A.E., Russell, J.L., Barrell, D.J.A., Schaefer, J.M., Kaplan, M.R., Strand, P.D., 2021. The Zealandia Switch: ice age climate shifts viewed from Southern Hemisphere moraines. Quaternary Science Reviews, 257, 106771.

DGA, 1987. Balance Hídrico de Chile. Direcci_on General de Aguas, Santiago, Chile.

Dortch, J.M., Owen, L.A., Caffee, M.W., 2013. Timing and climatic drivers for glaciation across semi-arid western Himalayan-Tibetan orogen. Quaternary Science Reviews 78, 188–208.

Doughty, A.M., Kaplan, M.R., Peltier, C., Barker, S., 2021. A maximum in global glacier extent during MIS 4 . Quaternary Science Reviews, 261, 106948

Doughty, A.M., Schaefer, J.M., Putnam, A.E., J.M, Denton, G.H., Kaplan, M.R., Barrell, D.J.A., Andersen, B.G., Kelley, S.E., Finkel, R.C., Schwartz, R., 2015. Mismatch of glacier extent and summer insolation in Southern Hemisphere mid-latitudes. Geology, 43, 407–410. https://doi.org/10.1130/G36477.1.

Evenson, E.B., Burkhart, P.A., Gosse, J.C., Baker, G.S., Jackofsky, D., Meglioli, A., Dalziel, I., Kraus, S., Alley, R.B., Berti, C., 2009. Enigmatic boulder trains, supraglacial rock avalanches, and the origin of ‘Darwin's boulders,’ Tierra del Fuego. GSA Today, 19, 4–10.

Fink, D., Williams, P.W., Augustinus, P., Shulmeister, J., 2006. Glacial chronologies across southern hemisphere latitudes during the past 30 ka and correlations to Antarctic ice cores. In: Burge, P.I., Shulmeister, J., Turney, C. (Eds.), Australasian INTIMATE Meeting. University of Auckland, pp. 14–16.

García, J. L., Hein, A. S., Binnie, S. A., Gomez, G. A., Gonzalez, M. A., Dunai, T. J., 2018. The MIS 3 maximum of the Torres del Paine and Última Esperanza ice lobes in Patagonia and the pacing of southern mountain glaciation. Quaternary Science Reviews, 185, 9–26.

García, J.-L., Lüthgens, C., Vega, R. M., Rodés, Á., Hein, A. S., Binnie, S. A. 2021. A composite ^{10}Be, IR-50 and ^{14}C chronology of the pre-Last Glacial Maximum (LGM) full ice extent of the western Patagonian Ice Sheet on the Isla de Chiloé, south Chile (42° S), E & G Quaternary Sci. J., 70, 105–128, https://doi.org/10.5194/egqsj-70-105-2021

García, J.L., 2012. Late Pleistocene ice fluctuations and glacial geomorphology of the Archipiélago de Chiloé, southern Chile. Geogr. Ann. 94, 459–479. doi: 10.1111/j.1468-0459.2012.00471.x

García, J.L., Hall, B.L., Kaplan, M.R., Vega, R.M., Strelin, J.A., 2014. Glacial geomorphology of the Torres del Paine region (southern Patagonia): implications for glaciation, deglaciation and paleolake history. Geomorphology 204, 599–616. https://doi.org/10.1016/j.geomorph.2013.08.036.

Garreaud, R.D., 2007. Precipitation and circulation covariability in the extratropics. J. Clim. 20, 4789–4797. https://doi.org/10.1175/JCLI4257.1

Gersonde, R., Crosta, X., Abelmann, A., Armand, L., 2005. Sea-surface temperature and sea ice distribution of the Southern Ocean at the EPILOG Last Glacial Maximum—a circum-Antarctic view based on siliceous microfossil records.

Quaternary Science Reviews, 24(7–9), 869–896.

Gillespie, A., Clark, D.H., 2011. Glaciations of the Sierra Nevada, USA. In: Ehlers, J., Gibbard, P.L., Hughes, P.D. (Eds.), Quaternary Glaciations — Extent and Chronology: A Closer Look. Developments in Quaternary Science, 15. Elsevier, Amsterdam, pp. 447–462.

Gillespie, A., Molnar, P. 1995. Asynchronous maximum advances of mountain and continental glaciers. Reviews of Geophysics, 33, 3, 311–364.

Girault, I., Todisco, D., Çiner, A., Sarıkaya, M.A., Yıldırım, C., Quiquerez, A., Martin, F., Borrero, L., Fabel, D., Grandjean, P., Nehme, C., Mouralis, D., 2022. 10Be chronology of deglaciation and ice-dammed lake regression in the vicinity of the Mylodon Cave (Cerro Benítez, Patagonia, Chile), Quaternary Science Reviews, 278, https://doi.org/10.1016/j.quascirev.2021.107354

Glasser, N. F., Clemmens, S., Schnabel, C., Fenton, C. R., McHargue, L., 2009. Tropical glacier advances in the Cordillera Blanca, Peru between 12.5 and 7.6 ka from cosmogenic 10Be dating. Quaternary Science Reviews, 28, 3448–3458.

Glasser, N. F., Jansson, K. N., Harrison, S., Klemen, J., 2008. The glacial geomorphology and Pleistocene history of Southern South America between 38°S and 56°S. Quaternary Science Reviews, 27, 365–390.

Gosse, J.C., Bell, T., Gray, J., 2006. Using cosmogenic isotopes to interpret the landscape record of glaciation: Nunataks in Newfoundland? In: Knight, P. (Ed.), Glacier Science and Environmental Change. Blackwell Publishing, 442–446.

Harrison, S., Glasser, N.F., 2011. Chapter 54 - The pleistocene glaciations of Chile. In: Jürgen Ehlers, P.L.G., Philip, D.H. (Eds.), Developments in Quaternary Sciences. Elsevier, pp. 739–756.

Hein, A.S., Cogez, A., Darvill, C.M., Mendelova, M., Kaplan, M.R., Herman, F.,

Dunai, T.J., Norton, K., Xu, S., Christl, M., 2017. Regional mid-Pleistocene glaciation in central Patagonia. Quaternary Science Reviews, 164, 77–94.

Hein, A.S., Dunai, T.J., Hulton, N.R.J., Xu, S., 2011. Exposure dating outwash gravels to determine the age of the greatest Patagonian glaciations. Geology, 39, 103–106.

Hein, A.S., Hulton, N.R., Dunai, T.J., Sugden, D.E., Kaplan, M.R., Xu, S., 2010. The chronology of the Last Glacial Maximum and deglacial events in central Argentine Patagonia. Quaternary Science Reviews, 29, 1212–1227.

Heusser, C.J., Heusser, L.E., Lowell, T.V., 1999. Paleo-ecology of the southern Chilean Lake District- Isla Grande de Chiloe- during middle-Late Llanquihue glaciation and deglaciation. Geogr. Ann., 81A, 231–284. https://doi.org/10.1111/1468-0459.00058.

Hjort, C., Ingolfsson, O., Bentley, M.G., Björck, S., 2003. The Late Pleistocene and Holocene glacial and climate history of the Antarctic Peninsula region as documented by the land and lake sediment records – A review. American Geophysical Union Antarctic Research Series, 79, 95–102.

Houmark-Nielsen, M., 2011. Pleistocene glaciations in Denmark: a closer look at chronology, ice dynamics and landforms. In: Ehlers, J., Gibbard, P.L., Hughes, P.D. (Eds.), Quaternary Glaciations — Extent and Chronology: A Closer Look. Developments in Quaternary Science, 15. Elsevier, Amsterdam, pp. 47–58.

Hughes, P. D., Gibbard, P. L., Ehlers, J., 2013. Timing of glaciation during the last glacial cycle: evaluating the concept of a global “Last Glacial Maximum”. Earth Sci. Rev., 125, 171–198.

Hughes, P., Fletcher, W., Bell, B. et al. 2020. Late Pleistocene glaciers to present-day snowpatches: a review and research recommendations for the Marrakech High

Atlas. Mediterranean Geoscience Reviews, 2, 163–184. https://doi.org/10.1007/s42990-020-00027-4

Hughes, P.D., Fink, D., Rodés, A., Fenton, C.R., Fujioka, G., 2018. Timing of Pleistocene glaciations in the High Atlas, Morocco: New ^{10}Be and ^{36}Cl exposure ages. Quaternary Science Reviews, 180, 193–213.

Hughes, P.D., Woodward, J.C. 2017. Quaternary glaciation in the Mediterranean mountains: a new synthesis. Geological Society London, Spec. Publ. 433, 1–23. https://doi.org/10.1144/SP433.14

Hulton, N., Purves, N., McCulloch, R., Sugden, D. E., Bentley, M. J. 2002. The Last Glacial Maximum and deglaciation in southern South America. Quaternary Science Reviews, 21, 233–241.

Ibarzabal y Donangelo, T., Hoffmann, J., Naruse, R., 1996. Recent climate changes in southern Patagonia, Bulletin of Glacier Research, 14, 29–36.

Ingolfsson, O. 2014. Late Quaternary Glaciation of Antarctica. Elsevier

James, L.A., Harbor, J., Fabel, D., Dahms, D., Elmore, D., 2002. Late Pleistocene glaciations in the Northwestern Sierra Nevada, California. Quaternary Research, 57, 409–419.

Jomelli, V., Favier, V., Vuille, M., Braucher, R., Martin, L., Blard, P.H., Colose, C., Brunstein, D., He, F., Khodri, M., Bourles, D.L., Leanni, L., Rinterknecht, V., Grancher, D., Francou, B., Ceballos, J.L., Fonseca, H., Liu, Z., Otto-Bliesner, B.L., 2014. A major advance of tropical Andean glaciers during the Antarctic cold reversal. Nature, 513 (7517), 224–228.

Kaplan M. R., Ackert, R. P., Singer, B. S., Douglass, D. C., Kurz, M. D., 2004. Cosmogenic nuclide chronology of millennial-scale glacial advances during O-isotope Stage 2 in Patagonia. Geological Society of America Bulletin, 116, 308–

321.

Kaplan, M.R., Coronato, A., Hulton, N.R.J., Rabassa, J.O., Kubik, P.W., Freeman, S.P.H.T., 2007. Cosmogenic nuclide measurements in southernmost South America and implications for landscape change. Geomorphology, 87, 284–301.

Kaplan, M.R., Fogwill, C.J., Sugden, D.E., Hulton, N.R.J., Kubik, P.W., Freeman, S.P.H.T., 2008. Southern Patagonian glacial chronology for the Last Glacial period and implications for Southern Ocean climate. Quaternary Science Reviews, 27, 284–294.

Kaplan, M.R., Strelin, J.A., Schaefer, J.M., Denton, G.H., Finkel, R.C., Schwartz, R., Putnam, A.E., Vandergoes, M.J., Goehring, B.M., Travis, S.G., 2011. In-situ cosmogenic 10Be production rate at Lago Argentino, Patagonia: implications for late-glacial climate chronology. Earth Planet. Sci. Lett., 309, 21–32.

Kelley, S.E., Kaplan, M.R., Schaefer, J.M., Andersen, B.G., Barrell, D.J.A., Putnam, A.E., Denton, G.H., Schwartz, R., Finkel, R.C., Doughty, A.M., 2014. High-precision 10Be chronology of moraines in the Southern Alps indicates synchronous cooling in Antarctica and New Zealand 42,000 years ago. Earth Planet Sci. Lett., 405, 194–206. https://doi.org/10.1016/j.epsl.2014.07.031.

Kilian, R., Baeza, O., Breuer, S., Rios, F., Arz, H., Lamy, F., Wirtz, J., Baque, D., Korf, P., Kremer, K., Ríos, C., Mutschke, E., Simon, M., De Pol-Holz, R., Arevalo, M., Worner, G., Schneider, C., Casassa, G., 2013. Late glacial and Holocene paleo-geographical and paleoecological evolution of the seno skyring and Otway fjord systems in the magellan region. An. Inst. Patagonia 41, 5–26.

Korschinek, G., Bergmaier, A., Faestermann, T., Gerstmann, U. C., Knie, K., Rugel, G., ... & Remmert, A. 2010. A new value for the half-life of 10Be by heavy-ion elastic recoil detection and liquid scintillation counting. Nuclear Instruments

and Methods in Physics Research Section B: Beam Interactions with Materials and Atoms, 268(2), 187–191.

Köse, O., Sarıkaya, M.A., Çiner, A., Candaş, A. 2019. Late Quaternary glaciations and cosmogenic ^{36}Cl geochronology of Mount Dedegöl, south-west Turkey. J. of Quaternary Science, 34, 1, 51–63. doi:10.1002/jqs.3080

Kuhlemann, J., Rohling, E.J., Krumrei, I., Kubik, P., Ivy-Ochs, S., Kucera, M., 2008. Regional synthesis of Mediterranean atmospheric circulation during the Last Glacial Maximum. Science, 321, 1338–1340.

Laabs, B.J.C., Refsnider, K.A., Munroe, J.S., Mickelson, D.M., Applegate, P.J., Singer, B.S., Caffee, M.W., 2009. Latest Pleistocene glacial chronology of the Uinta Mountains: support for moisture-driven asynchrony of the last deglaciation. Quaternary Science Reviews, 28, 1171–1187.

Lal, D., 1991. Cosmic ray labeling of erosion surfaces: in situ nuclide production rates and erosion models. Earth and Planetary Science Letters, 104(2–4), 424–439.

Larter, R.D., Anderson, J.B., Graham, A.G.C., Gohl, K., Hillenbrand, C.-D., Jakobsson, M., Johnson, J.S., Kuhn, G., Nitsche, F.O., Smith, J.A., Witus, A.E., Bentley, M.J., Dowdeswell, J.A., Ehrmann, W., Klages, J.P., Lindow, J., O ´ Cofaigh, C., Spiegel, C., 2014. Reconstruction of changes in the Amundsen Sea and Bellingshausen Sea sector of the West Antarctic Ice Sheet since the Last Glacial Maximum. Quaternary Science Reviews, 100, 55– 86.

Leontaritis, A.D., Kouli, K., Pavlopoulos, K. 2020. The glacial history of Greece: a comprehensive review. Mediterranean Geoscience Reviews, 2, 65–90. https://doi.org/10.1007/s42990-020-00021-w

Licciardi, J.M., Pierce, K.L., 2008. Cosmogenic exposure age chronologies of Pinedale and Bull Lake glaciations in greater Yellowstone and the Teton Range,

USA. Quaternary Science Reviews, 27, 814–831.

Lifton, N., Sato, T., Dunai, T. J., 2014. Scaling in situ cosmogenic nuclide production rates using analytical approximations to atmospheric cosmic-ray fluxes. Earth and Planetary Science Letters, 386, 149–160.

Mangerud, J., Gyllencreutz, R., Øystein, L., Svendsen, J.I., 2011. Glacial history of Norway. In: Ehlers, J., Gibbard, P.L., Hughes, P.D. (Eds.), Quaternary Glaciations — Extent and Chronology: A Closer Look. Developments in Quaternary Science, 15. Elsevier, Amsterdam, pp. 279–298.

Martin, F. M., San Román, M., Morello, F., Todisco, D., Prevosti, F. J., Borrero, L. A., 2013. Land of the ground sloths: recent research at Cueva Chica, Ultima Esperanza, Chile. Quaternary International, 305, 56–66.

McCarthy, A., Mackintosh, A., Rieser, U., Fink, D., 2008. Mountain glacier chronology from Boulder Lake, New Zealand, indicates MIS 4 and MIS 2 ice advances of similar extent. Arctic Antarct. Alpine Res., 40, 695–708. https://doi.org/10.1657/1523-0430(06-111)[MCCARTHY]2.0.CO;2.

McCulloch, R. D. , Fogwill, C. J., Sugden, D. E., Bentley, M. J., Kubik, P. W. 2005. Chronology of the Last Glaciation in Central Strait of Magellan and Bahía Inútil, Southernmost South America , Geografiska Annaler. Series A, Physical Geography, 87, 2, 289–312

Meglioli, A., 1992. Glacial geology and chronology of Southernmost Patagonia and Tierra del Fuego, Argentina and Chile (PhD Thesis). Lehigh University, Pennsylvania, 215 p.

Mendelova, M., Hein, A., McCulloch, R., Davies, B., 2017. The Last Glacial Maximum and Deglaciation in Central Patagonia, 44º S–49º S. Cuadernos de Investigación Geográfica, 43, 719.

Mendelova, M., Hein, A., Rod, A., Xu, S., 2020. Extensive mountain glaciation in central Patagonia during Marine Isotope Stage 5. Quaternary Science Reviews, 227, 105996.

Mercer, J.H., 1984. Simultaneous climatic change in both hemispheres and similar bipolar interglacial warming: evidence and implications. In: Hansen, J.E., Takahashi, T. (Eds.), Climate Processes and Climate Sensitivity, vol. 29. American Geophysical Union, Washington, D. C., pp. 307–313 of Geophysical Monograph Series.

Mix, A.C., Bard, E., Schneider, R. 2001. Environmental processes of the ice age: land, oceans, glaciers (EPILOG). Quaternary Science Reviews, 20, 627–657.

Monegato, G., Scardia, G., Rizzini, F., Piccin, A. 2017. The Alpine LGM in the boreal icesheets Game. Scientific Reports, 7: 2078, Doi:10.1038/s41598-017-02148-7

Moreno, F. P., 1899. Explorations in Patagonia. The Geographical Journal, 14(3), 241–269.

Moreno, P.I., Denton, G.H., Moreno, H., Lowell, T.V., Putnam, A.E., Kaplan, M.R., 2015. Radiocarbon chronology of the Last Glacial Maximum and its termination in northwestern Patagonia. Quaternary Science Reviews, 122, 233–249.

Nyvlt, D., Glasser, N.F., Hocking, E., Oliva, M., Roberts, S.J., Roman, M. 2020. Tracing the deglaciation since the Last Glacial Maximum. In: Past Antarctica, Oliva et al (eds). Chapter 5.

Ó'Cofaigh, C., Davies, B.J., Livingstone, S.J., Smith, J.A., Johnson, J.S., Hocking, E.P., et al. 2014. Reconstruction of ice-sheet changes in the Antarctic Peninsula since the Last Glacial Maximum. Quaternary Science Reviews, 100, 87–110.

Oerlemans, J. (2005). Extracting a climate signal from 169 glacier records. Science, 308, 675–677.

Oliva, M., Palacios, D., Fernández-Fernández, J.M. et al., 2019. Late Quaternary glacial phases in the Iberian Peninsula, Earth-Science Reviews, https://doi.org/10.1016/j.earscirev.2019.03.015

Owen, L. A., Dortch, J. M., 2014. Nature and timing of Quaternary glaciation in the Himalayan-Tibetan orogen. Quaternary Science Reviews, 88, 14–54.

Owen, L., Caffee, M., Finkel, R. Seong, Y. B., 2008. Quaternary glaciation of the Himalayan-Tibetan orogen. Journal of Quaternary Science, 23, 513–531.

Palacios, D., Stokes, C.R., Phillips, F.M., Clagued, J.J., Alcalá–Reygosa, J., Andrés, N., Angel, I., Blard, P–H., Briner, J.P., Hall, B.L., Dahms, D., Hein, A.S., Jomelli, V., Mark, B.G., Martini, M.A., Moreno, P. Riedel, J., Sagredo, E., Stansell, N.D., Vázquez–Selem, L., Vuille, M., Ward, D.J. 2020. The deglaciation of the Americas during the Last Glacial Termination. Earth–Science Reviews, 203, 103113. https://doi.org/10.1016/j.earscirev.2020.103113

Peltier, C., Kaplan, M.R., Birkel, S.D., Soteres, R.L., Sagredo, E.A., Aravena, J.C., Araos, J., Moreno, P.I., Schwartz, R., Schaefer, J.M., 2021. The large MIS 4 and long MIS 2 glacier maxima on the southern tip of South America. Quaternary Science Reviews, 94-106.

Philips, F., Zreda, M., benson, L.V., Plummer, M.A., Elmore, D., Sharma, P. 1996. Chronology for Fluctuationsin Late Pleistocene Sierra Nevada Glaciers and Lakes, Science, 274(5288), 749–751.Doi:10.1126/science.274.5288.749

Phillips, F.M., Zreda, M.G., Smith, S.S., Elmore, D., Kubik, P.W., Sharma, P. 1990. Cosmogenic chlorine-36 chronology for glacial deposits at Bloody Canyon, eastern Sierra Nevada, Science, 248, 1529–1532.

Putnam, A.E., Schaefer, J.M., Denton, G.H., Barrell, D.J.A., Birkel, S.D., Andersen, B.G., Kaplan, M.R., Finkel, R.C., Schwartz, R., Doughty, A.M., 2013. The last glacial maximum at 44ºS documented by a ^{10}Be moraine chronology at lake Ohau, southern Alps of New Zealand. Quaternary Science Reviews, 62, 114–141. https://doi.org/10.1016/j.quascirev.2012.10.034.

Quirk, B.J., Moore, J.R., Laabs, B.J.C., Plummer, M.A., Caffee, M.W. 2020. Latest Pleistocene glacial and climate history of the Wasatch Range, Utah. Quaternary Science Reviews, 238, 106313.

Rabassa, J., 2008. Late Cenozoic glaciations in Patagonia and Tierra del Fuego. In: Rabassa, J. (Ed.), Late Cenozoic of Patagonia and Tierra del Fuego. Developments in Quaternary Sciences, 11, Elsevier, Amsterdam, 151–204.

Rabassa, J., Coronato, A. 2009. Glaciations in Patagonia and Tierra del Fuego during the Ensenadan Stage/Age (Early Pleistocene–earliest Middle Pleistocene). Quaternary International, 210, 18–36.

Rabassa, J., Coronato, A., Martinez, O., Reato, A. 2022. Last Glacial Maximum, Late Glacial and Holocene of Patagonia. In: Archaeology of Piedra Museo Locality: An open window to the early population of Patagonia. Springer, pp. 59–84.

RAISED Consortium, et al., 2014. A community-based geological reconstruction of Antarctic Ice Sheet deglaciation since the Last Glacial Maximum. Quaternary Science Reviews, 100, 1–9.

Rhee, H.H., Lee, M.K., Seong, Y.B., Hong, S., Lee, J.I., Yoo, K-C, Yu, B.Y., 2019. Timing of the local last glacial maximum in Terra Nova Bay, Antarctica defined by cosmogenic dating. Quaternary Science Reviews, 221, 105897.

Rother, H., Stauch, G., Loibl, D., Lehmkuhl, F., Freeman, S. P. H. T., 2017. Late Pleistocene glaciations at Lake Donggi Cona, eastern Kunlun Shan (NE Tibet):

early maxima and a diminishing trend of glaciation during the last glacial cycle. Boreas, 10.1111/bor.12227. ISSN 0300-9483.

Sagredo, E. A., Moreno, P. I., Villa-Martinez, R., Kaplan, M. R., Kubik, P. W., Stern, C. R., 2011. Fluctuations of the Última Esperanza ice lobe (52°S), Chilean Patagonia, during the last glacial maximum and termination. Geomorphology, 125, 92–108.

Sarıkaya, M.A., Çiner, A. 2015. Late Pleistocene glaciations and paleoclimate of Turkey. Bull. of Mineral Research and Exploration, 151, 107–127.

Sarıkaya, M.A., Çiner, A. 2017. The late Quaternary glaciation in the Eastern Mediterranean. In: "Quaternary Glaciation in the Mediterranean Mountains". Hughes, P. & Woodward, J. (eds.), Geological Society of London Special Publication, 433, 289–305, doi:10.1144/SP433.4

Sarıkaya, M.A., Çiner, A., Haybat, H., Zreda, M. 2014. An early advance of glaciers on Mount Akdağ, SW Turkey, before the global Last Glacial Maximum; insights from cosmogenic nuclides and glacier modeling. Quaternary Science Reviews, 88, 96–109. doi:10.1016/j.quascirev.2014.01.016

Sarıkaya, M.A., Stepišnik, U., Žebre, M., Çiner, A., Yıldırım, C., Vlahovic, I., Tomljenovic, B., Matos, B., Wilcken, K.M. 2020. Last glacial maximum deglaciation of the Southern Velebit Mt. (Croatia): insights from cosmogenic 36Cl dating of Rujanska Kosa. Mediterranean Geoscience Reviews, 2, 1, 53–64. doi:10.1007/s42990-020-00030-9

Sarıkaya, M.A., Zreda, M. Çiner, A. 2009. Glaciations and palaeoclimate of Mt Erciyes, central Turkey, since the Last Glacial Maximum, inferred from ^{36}Cl cosmogenic dating and glacier modeling. Quaternary Science Reviews, 28 (23–24), 2326–2341.

Sarıkaya, M.A., Zreda, M., Çiner, A., Zweck, C. 2008. Cold and wet Last Glacial Maximum on Mount Sandıras, SW Turkey, inferred from cosmogenic dating and glacier modeling. Quaternary Science Reviews, 27, 7–8, 769–780. doi:10.1016/j.quascirev.2008.01.002.

Schaefer, J.M., et al., 2015. The southern glacial maximum 65,000 years ago and its unfinished termination. Quaternary Science Reviews, 114, 52–60. https://doi.org/10.1016/j.quascirev.2015.02.009.

Seguinot, J., Ivy-Ochs, S., Jouvet, G., Huss, M., Funk, M., Preusser, F. 2018. Modelling last glacial cycle ice dynamics in the Alps. The Cryosphere, 12, 3265–3285, https://doi.org/10.5194/tc-12-3265-2018

Shulmeister, J., Thackray, G.D., Rittenour, T.M., Fink, D., Patton, N.R., 2019. The timing and nature of the last glacial cycle in New Zealand. Quaternary Science Reviews, 206, 1–20.

Solari, M., Le Roux, J., Herve_, F., Airo, A., Caldero_n, M., 2012. Evolution of the Great Tehuelche Paleolake in the Torres del Paine National Park of Chilean Patagonia during the Last Glacial Maximum and Holocene. Andean Geol., 39, 1–21.

Stern, C. R., Moreno, P. I., Villa-Martinez, R., Sagredo, E. A., Prieto, A., Labarca, R., 2011. Evolution of ice-dammed proglacial lakes in Última Esperanza, Chile: implications from the late-glacial R1 eruption of Reclús volcano, Andean Austral Volcanic Zone. Andean Geology, 38(1), 82–97.

Stokes, C., Tarasov, L., Dyke, A.S., 2012. Dynamics of the north American Ice Sheet Complex during its inception and build-up to the Last Glacial Maximum. Quaternary Science Reviews, 50, 86–104.

Stone, J. O., 2000. Air pressure and cosmogenic isotope production. Journal of

Geophysical Research, 105(B10), 23,753–23,759.

Stone, J. O., Balco, G. A., Sugden, D. E., Caffee, M. W., Sass, L. C., Cowdery, S. G., Siddoway, C., 2003. Holocene deglaciation of Marie Byrd land, west Antarctica. Science, 299, 99–102.

Sugden, D.E., Bentley, M.J., Fogwill, C.J., Hulton, N.R.J., Mcculloch, R.D., Purves, R.S. 2005. Late- glacial glacier events in southernmost south america: a blend of 'northern' and 'southern' hemispheric climatic signals? Geografiska Annaler: Series A, Physical Geography, 87:2, 273–288. https://doi.org/10.1111/j.0435-3676.2005.00259.x

Sutherland, R., Kim, K., Zondervan, A., McSaveney, M., 2007. Orbital forcing of midlatitude Southern Hemisphere glaciation since 100 ka inferred from cosmogenic nuclide ages of moraine boulders from the Cascade Plateau, southwest New Zealand. Geol. Soc. Am. Bull., 119 (3/4), 443–451. https://doi.org/10.1130/B25852.1.

Thackray, G.D., 2008. Varied climatic and topographic influences on Late Pleistocene mountain glaciation in the western United States. Journal of Quaternary Science, 23, 671–681.

Ünal-İmer, E., Shulmeister, J., Zhao, J-X., Uysal, T., Feng, Y-X., Nuguyen, A.I., Yüce, G., 2015. An 80 kyr-long continuous speleothem record from Dim Cave, SW Turkey with paleoclimatic implications for the Eastern Mediterranean. Sci. Reports, 5, 13560; doi: 10.1038/srep13560

Wright, A.P, White, D.A., Gore, D.B., Siegert, M.J. 2008. Antarctica at the Last Glacial Maximum, Deglaciation and the Holocene. In: Antarctic climate evolution. F. Florindo and M. Siegert (Eds.). Developments in Earth & Environmental Sciences, 8, 531–570. Doi:10.1016/S1571-9197(08)00012-8

Xu, S., Dougans, A. B., Freeman, S. P. H. T., Schnabel, C., Wilcken, K. M., 2010. Improved ^{10}Be and ^{26}Al AMS with a 5 MV spectrometer. Nuclear Instruments and Methods in Physics Research Section B: Beam Interactions with Materials and Atoms, 268(7–8), 736–738.

Žebre, M., Sarıkaya, M.A., Stepišnik, U., Colluci, R.R., Yıldırım, C., Çiner, A., Candaş, A., Vlahovic, I., Tomljenovic, B., Matos, B., Wilcken, K.M. 2021. An early glacial maximum during the last glacial cycle on the northern Velebit Mt. (Croatia), Geomorphology, 392, https://doi.org/10.1016/j.geomorph.2021.107918

Žebre, M., Sarıkaya, M.A., Stepišnik, U., Yıldırım, C., Çiner, A. 2019. First ^{36}Cl cosmogenic moraine geochronology of the Dinaric mountain karst: Velež and Crvanj Mountains of Bosnia and Herzegovina. Quaternary Science Reviews, 208, 54–75. doi:10.1016/j.quascirev.2019.02.002

Žebre, M., Sarıkaya, M.A., Stepišnik, U., Yıldırım, C., Çiner, A. 2019. First ^{36}Cl cosmogenic moraine geochronology of the Dinaric mountain karst: Velež and Crvanj Mountains of Bosnia and Herzegovina. Quaternary Science Reviews, 208, 54–75. doi: 10.1016/j.quascirev.2019.02.002.

Figures and Tables

Fig. 1: Study area location and geomorphological map: Insert: Patagonian Ice Sheet extent during the gLGM and Present. B: Geomorphological map of the Última Esperanza ice-lobe moraine complexes modified from Sagredo et al. (2011), García et al. (2014, 2018) and Girault et al. (2022). Sagredo et al. (2011) cores and sections: a: Lago Dorotea pit; b: Vega Benítez pit; c: Eberhard pit; Dorotea pits section; e: Dumestre section; f: Pantano Dumestre pit; g: Lago Pintito pit.

Fig. 2: Field pictures from Aníbal Pinto moraine complex: A) Aníbal Pinto Lake view towards the southwest. B) Boulder trains composed of erratics on flattened moraine surface. C); Glacially sculpted bedrock wall. D) Lago Pintito, a small lake developed after the ice retreat in between moraine ridges.

Fig. 3: Erratic boulder samples and their corresponding ^{10}Be TCN ages.

Fig. 4: Moraine boulder ^{10}Be TCN exposure ages *vs* elevation graph (lower part). Probability density function (PDF), weighted average age of the exposure events (upper part). Coloured thin lines are individual ages from corresponding moraines (see map), and the coloured thick line is the summed probability curve. Purple: Río Turbio; Dashed pink: Arauco (outlier); Pink: Dos Lagunas (Arauco); Light brown: Cerro Benítez (Aníbal Pinto).

Fig. 5: Deglaciation scenario of the Última Esperanza ice-lobe from local to global LGM. For Legend see Fig. 1. 1) lLGM Río Turbio advance: 50.7 ± 2.4 ka (45.7 ± 1.3 ka; García et al., 2018). 2) Arauco advance (32.4 ± 1.1 ka; García et al., 2018), including the deposition of the Dos Lagunas moraine: (32.6 ± 2.2 ka; this study and 36.0 ± 1.0 ka; Sagredo et al., 2011). 3) Probable synchronous development of the Cerro Ballena moraine complex and the Aníbal Pinto moraine complex (28.3 ± 2.2 ka; this study) in the south. 4) Total drainage of Lago Consuelo showing present-day topography.

Table 1: Cosmogenic age data used in this study. Ages have been calculated using the online exposure age calculator formerly known as the CRONUS Earth Web Calculator v3 (https://hess.ess.washington.edu; Balco et al., 2008) with the mean attenuation length of 152.1 g/cm^2, rock density of 2.65 g/cm^3 and the Lifton/Sato flux, time and nuclide-dependent scaling scheme (known as LSDn, or SA) based on Lifton

et al. (2014). Choice of a different scaling scheme (i.e., Lal/Stone time-independent, ST) (Lal, 1991; Stone, 2000) would make the ages <2.4% older. Procedural blank correction applied. No snow or erosion correction was applied. Isotope ratios were referenced to the 07KNSTD standard.

Supplementary Table 1: Compilation of ^{10}Be surface exposure ages of erratic blocks from the area of the Última Esperanza ice lobe, except for those identified by the authors as outliers. ^{10}Be ages surface exposure ages from Sagredo et al. (2011), and García et al. (2018) were recalculated with different production rates and scaling schemes. We used the online exposure age calculator CRONUS v3 (https://hess.ess.washington.edu; Balco et al., 2008). Erosion was neglected, and snow correction was not applied, agreeing with Sagredo et al. (2011) and García et al. (2018). * Production rate and scaling scheme used in the discussion.

Supplementary Table 2: Ancillary data (e.g., carrier data, mass dissolved, beryllium isotope ratios from AMS, blank corrections, scaling factors, etc.) to recalculate the ^{10}Be TCN exposure ages.

Table 1

Sample	Glacial stage (or event)	Latitude WGS-84 (S)	Longitude WGS-84 (W)	Elevation (m asl)	Thickness (cm)	Topographic shielding factor unitless	Quartz dissolved (g)	^{10}Be conc. (at g^{-1})	1 σ error (at g^{-1})	**^{10}Be age (ka)**	1 σ error^{int} (ka)	**1 σ error$^{ext.}$ (ka)**	**Weighted average age (ka)**
ESP17-04	Rio Turbio advance	-52.0187	-71.9592	206	2	1	14.539	285000.7	7166.6	**51.8**	1.3	**3.4**	
ESP17-05	Rio Turbio advance	-52.0220	-71.9667	214	3	1	5.203	261189.8	9546.4	**47.3**	1.8	**3.3**	**50.7 ± 2.4**
ESP17-06	Rio Turbio advance	-52.0257	-71.9648	198	1	1	0.964	295813.4	22498.3	**53.8**	4.2	**5.3**	
ESP17-02	Arauco advance*?	-51.7887	-72.2039	184	4	1	3.378	226235.6	9814.3	***42.6****	*1.9**	***3.2****	
CRB17-12	Arauco advance (Dos Lagunas)	-51.5008	-72.4957	266	1.5	0.999	6.948	189026.9	5657.8	**32.6**	1.0	**2.2**	
ESP17-12	Regression of Lago Consuelo	-51.9909	-72.3721	145	2	1	7.884	98169.3	4667.2	**19.0**	0.9	**1.5**	**18.9 ± 1.0**
ESP17-14	Regression of Lago Consuelo	-52.0113	-72.3676	169	2	1	9.677	98812.6	3762.9	**18.7**	0.7	**1.3**	
ESP17-13	Anibal Pinto advance	-52.0420	-72.3776	188	3	0.999	10.290	152086.0	7656.0	**28.3**	1.4	**2.2**	

Figure 1

Click here to access/download;Figure (Color);Fig. 1.png

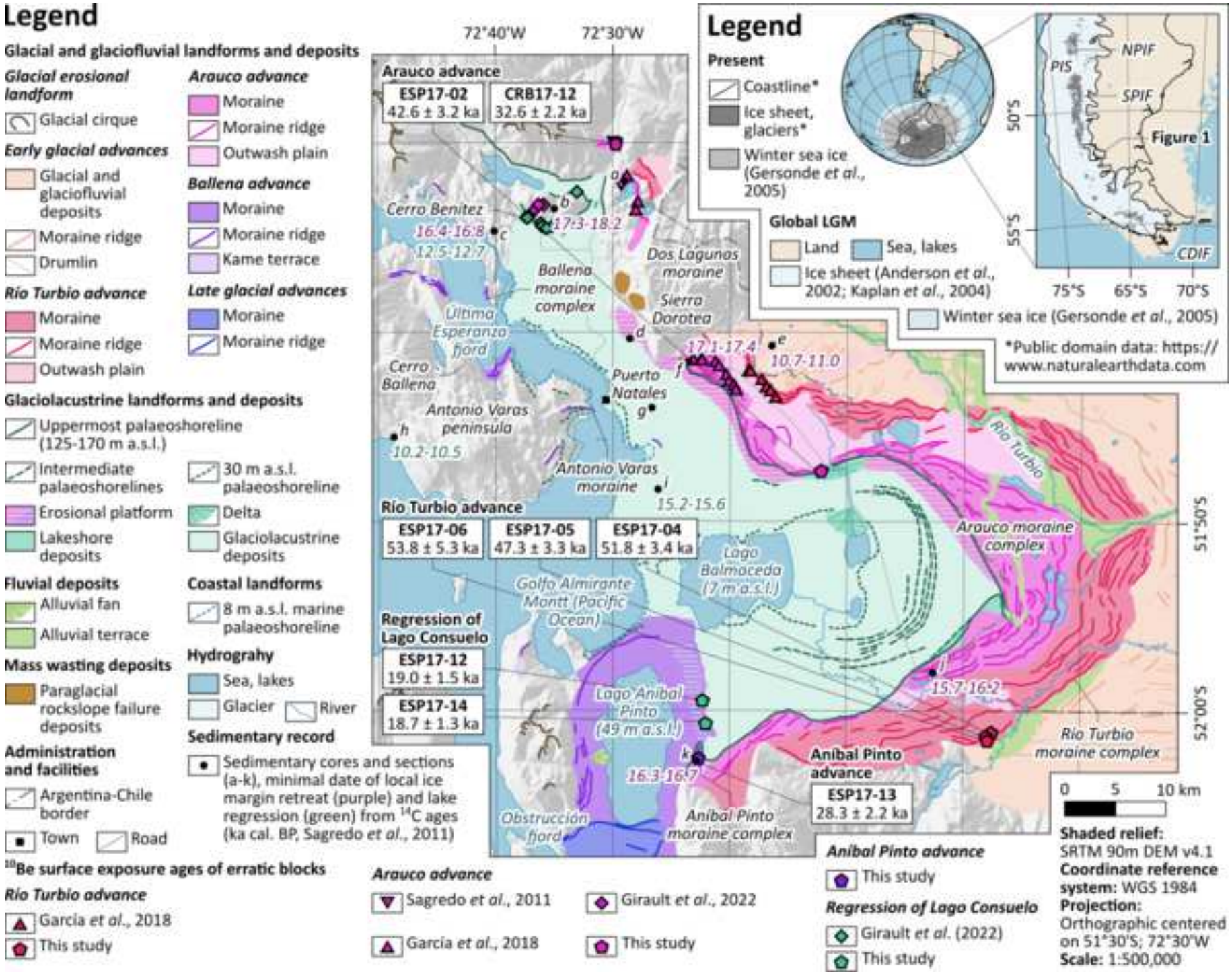

Figure 2

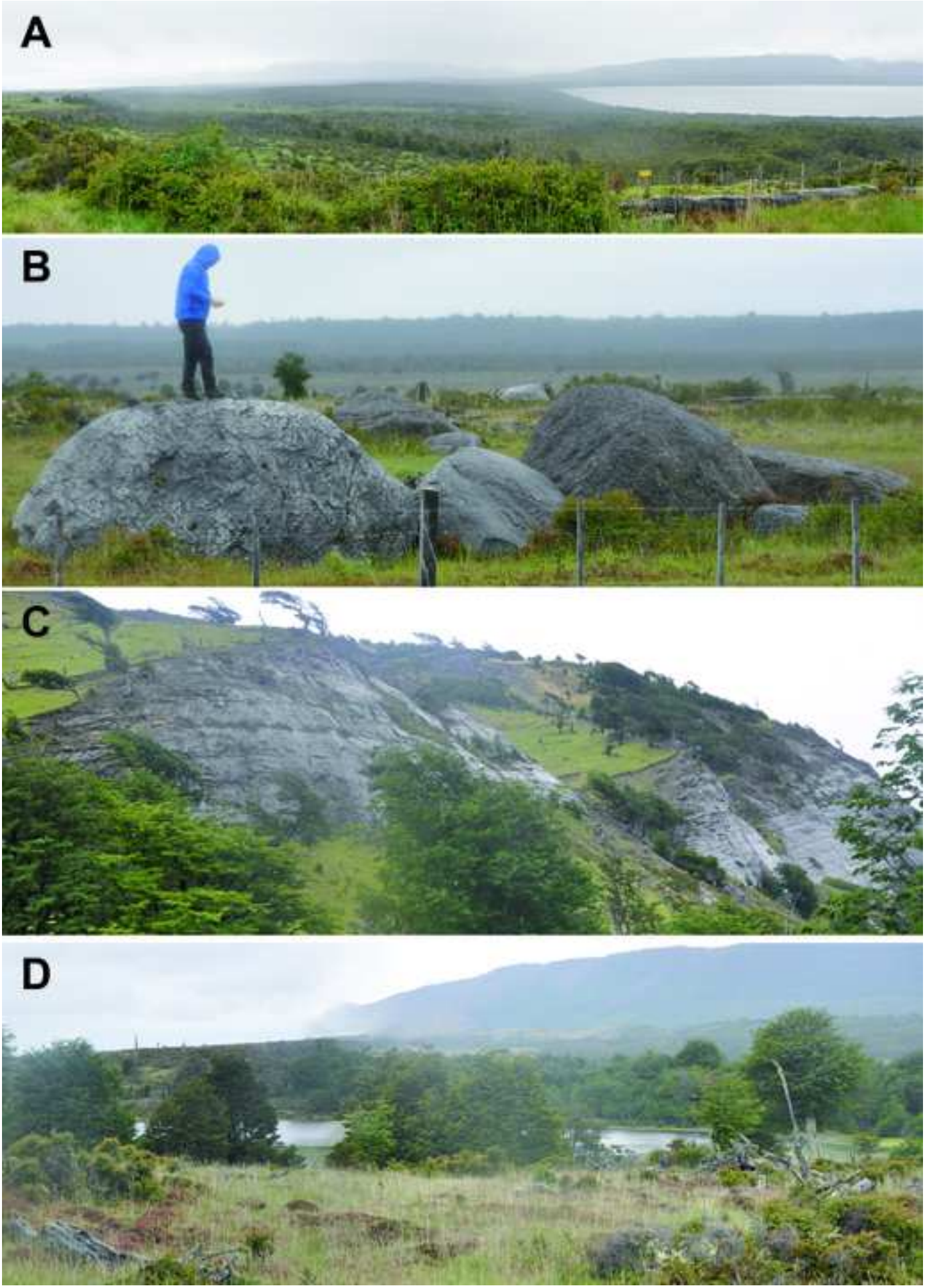

Figure 3

Click here to access/download;Figure (Color);Fig. 3.png

Figure 4

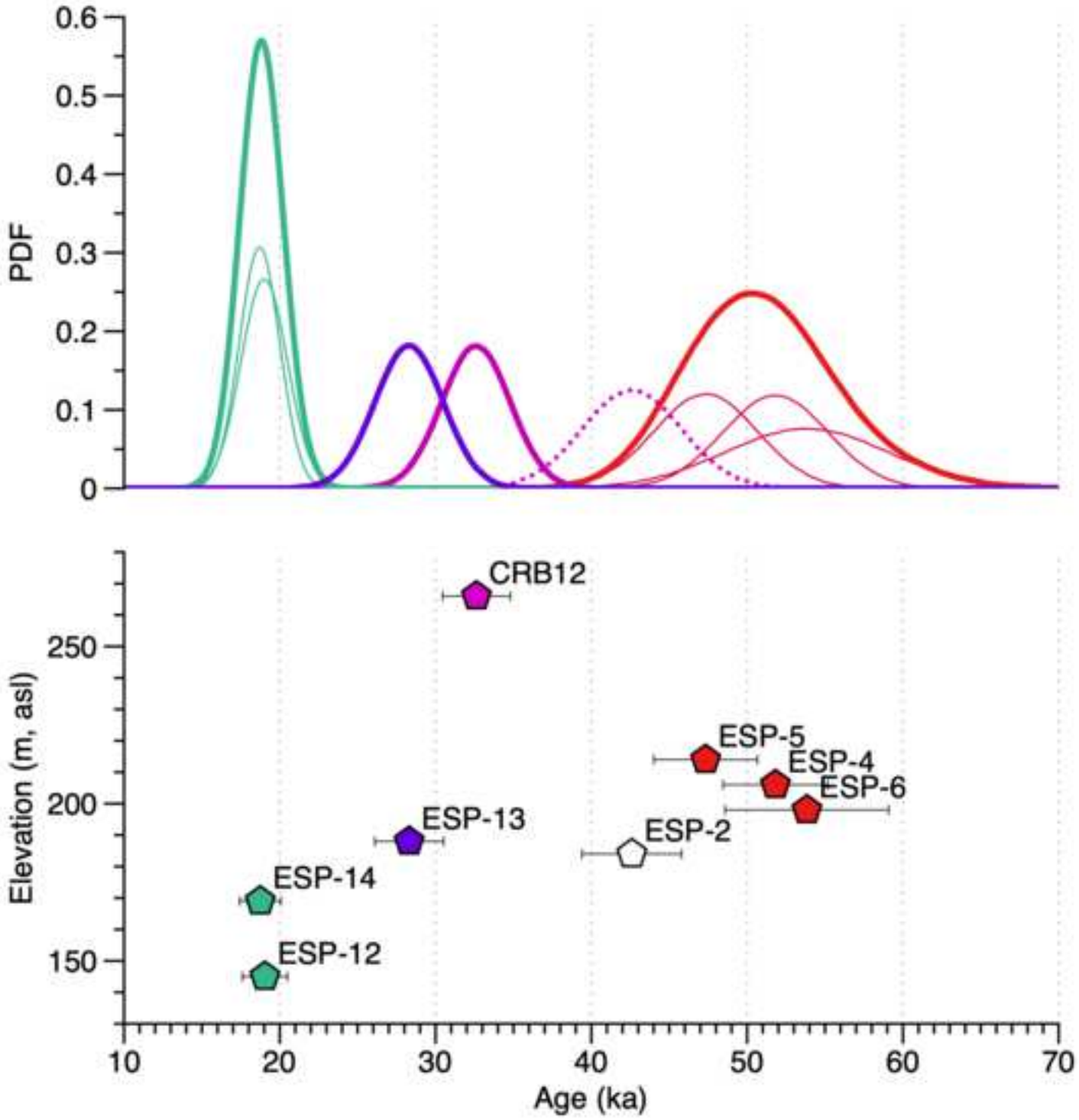

Figure 5

Click here to access/download;Figure (Color);Fig. 5.png

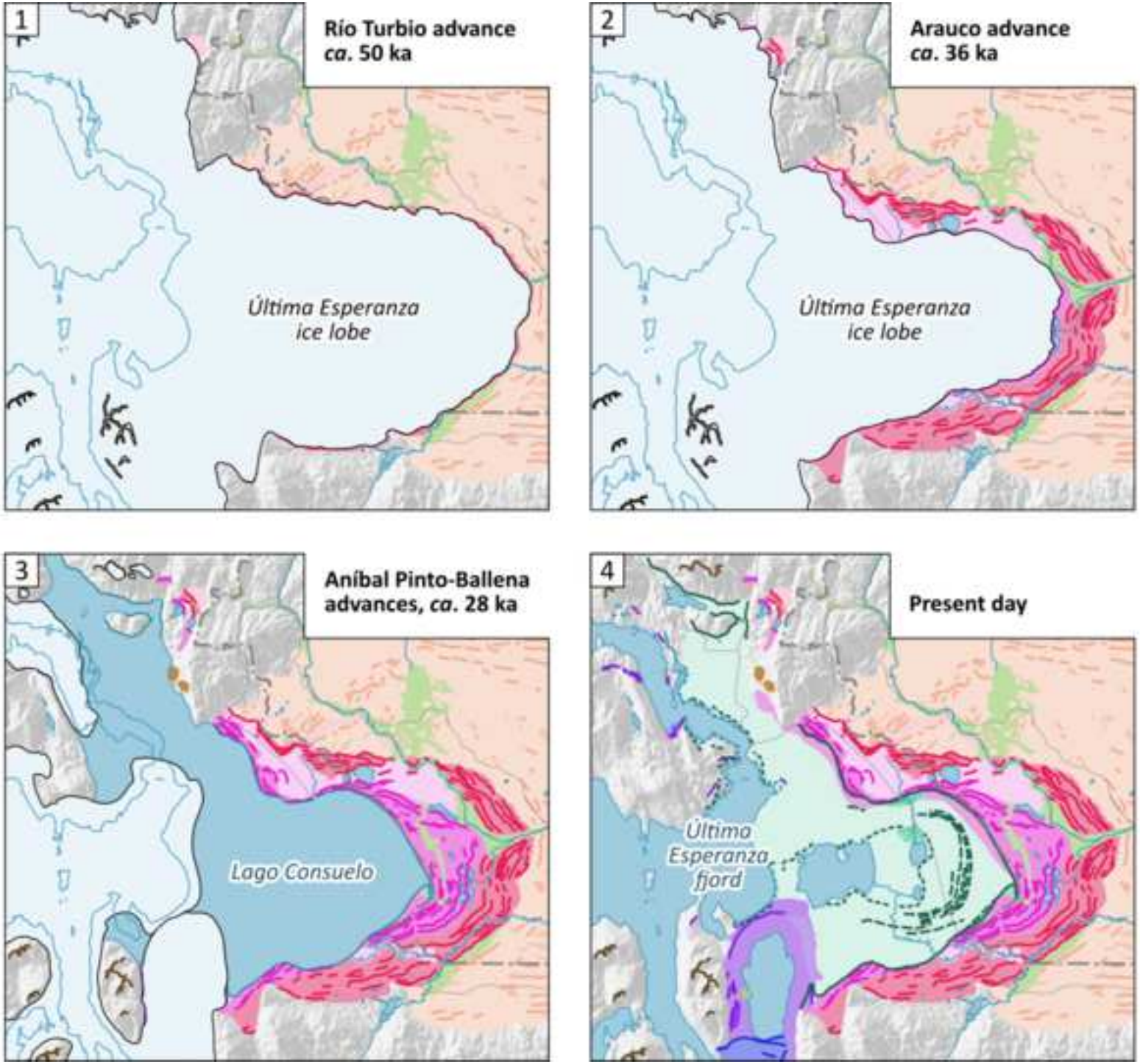

Declaration of interests

☐The authors declare that they have no known competing financial interests or personal relationships that could have appeared to influence the work reported in this paper.

☒The authors declare the following financial interests/personal relationships which may be considered as potential competing interests:

Fabiana Martin reports financial support was provided by FONDECYT (Chile). Dominique Todisco reports financial support was provided by CNRS PICS project GEOCEBE. Attila Ciner reports financial support was provided by Istanbul Technical University TGA-2017-40610. Attila Ciner reports a relationship with Istanbul Technical University that includes: employment.